Global Biogeochemical Cycles

RESEARCH ARTICLE
10.1029/2023GB007862

Special Section:
Regional Carbon Cycle Assessment and Processes - 2

An Assessment of CO_2 Storage and Sea-Air Fluxes for the Atlantic Ocean and Mediterranean Sea Between 1985 and 2018

Fiz F. Pérez[1], M. Becker[2], N. Goris[3], M. Gehlen[4], M. López-Mozos[1], J. Tjiputra[3], A. Olsen[2], J. D. Müller[5], I. E. Huertas[6], T. T. T. Chau[4], V. Cainzos[7], A. Velo[1], G. Benard[4], J. Hauck[8], N. Gruber[5], and Rik Wanninkhof[9]

[1]Instituto de Investigaciones Marinas (IIM), CSIC, Vigo, Spain, [2]Geophysical Institute, University of Bergen and Bjerknes Centre for Climate Research, Bergen, Norway, [3]NORCE Climate & Environment, Bjerknes Centre for Climate Research, Bergen, Norway, [4]Laboratoire des Sciences du Climat et de l'Environnement, LSCE/IPSL, CEA-CNRS-UVSQ, Université Paris-Saclay, Gif-sur-Yvette, France, [5]Environmental Physics, Institute of Biogeochemistry and Pollutant Dynamics, ETH Zurich, Zürich, Switzerland, [6]Instituto de Ciencias Marinas de Andalucía (ICMAN-CSIC), Cadiz, Spain, [7]Unidad Océano y Clima, Instituto de Oceanografía y Cambio Global, IOCAG, Universidad de Las Palmas de Gran Canaria, ULPGC, Unidad Asociada ULPGC-CSIC, Canary Islands, Spain, [8]Alfred-Wegener-Institut, Helmholtz-Zentrum für Polar- und Meeresforschung, Bremerhaven, Germany, [9]Atlantic Oceanographic and Meteorological Laboratory, National Oceanic and Atmospheric Administration, Miami, FL, USA

Key Points:

- From 1985 to 2018, pCO_2 products suggest a lower mean CO_2 uptake (-0.36 ± 0.06 PgC yr^{-1}) than ocean models (-0.47 ± 0.15 PgC yr^{-1})
- Since 2000, the CO_2 uptake is increasing twice as fast in the pCO_2 products compared to the models
- Major differences between models and pCO_2 products are attributed to the outgassing of riverine carbon and the seasonal cycle of pCO_2

Supporting Information:

Supporting Information may be found in the online version of this article.

Correspondence to:

F. F. Pérez and M. López-Mozos,
fiz.perez@iim.csic.es;
mlopezm@iim.csic.es

Citation:

Pérez, F. F., Becker, M., Goris, N., Gehlen, M., López-Mozos, M., Tjiputra, J., et al. (2024). An assessment of CO_2 storage and sea-air fluxes for the Atlantic Ocean and Mediterranean Sea between 1985 and 2018. *Global Biogeochemical Cycles*, *38*, e2023GB007862. https://doi.org/10.1029/2023GB007862

Received 30 MAY 2023
Accepted 25 MAR 2024
Corrected 3 JUN 2024

This article was corrected on 3 JUN 2024. See the end of the full text for details.

Author Contributions:

Conceptualization: Fiz F. Pérez, M. Becker, M. Gehlen, M. López-Mozos, J. Tjiputra, A. Olsen, J. D. Müller, I. E. Huertas, J. Hauck, N. Gruber, Rik Wanninkhof

Abstract

As part of the second phase of the Regional Carbon Cycle Assessment and Processes project (RECCAP2), we present an assessment of the carbon cycle of the Atlantic Ocean, including the Mediterranean Sea, between 1985 and 2018 using global ocean biogeochemical models (GOBMs) and estimates based on surface ocean carbon dioxide (CO_2) partial pressure (pCO_2 products) and ocean interior dissolved inorganic carbon observations. Estimates of the basin-wide long-term mean net annual CO_2 uptake based on GOBMs and pCO_2 products are in reasonable agreement (-0.47 ± 0.15 PgC yr^{-1} and -0.36 ± 0.06 PgC yr^{-1}, respectively), with the higher uptake in the GOBM-based estimates likely being a consequence of a deficit in the representation of natural outgassing of land derived carbon. In the GOBMs, the CO_2 uptake increases with time at rates close to what one would expect from the atmospheric CO_2 increase, but pCO_2 products estimate a rate twice as fast. The largest disagreement in the CO_2 flux between GOBMs and pCO_2 products is found north of 50°N, coinciding with the largest disagreement in the seasonal cycle and interannual variability. The mean accumulation rate of anthropogenic CO_2 (C_{ant}) over 1994–2007 in the Atlantic Ocean is 0.52 ± 0.11 PgC yr^{-1} according to the GOBMs, 28% ± 20% lower than that derived from observations. Around 70% of this C_{ant} is taken up from the atmosphere, while the remainder is imported from the Southern Ocean through lateral transport.

Plain Language Summary

This study contributes to the second Regional Carbon Cycle Assessment and Processes project by presenting a carbon cycle evaluation of the Atlantic Ocean including the Mediterranean Sea between 1985 and 2018. The assessment draws on output from global ocean biogeochemical models along with estimates based on observations of surface ocean carbon dioxide (CO_2) partial pressure (pCO_2 products) and ocean interior dissolved inorganic carbon. The models suggest that the Atlantic took up -0.47 ± 0.15 Pg of carbon per year, in reasonable agreement with an uptake of -0.36 ± 0.06 Pg carbon per year computed from pCO_2 products. In the models, the rate of CO_2 uptake is keeping pace with the increase in atmospheric CO_2, but it is twice as fast in the pCO_2 products. Most of the uptake of CO_2 by the ocean occurs in response to excess CO_2 released into the atmosphere from human activities. The so-called anthropogenic carbon accumulates in the Atlantic Ocean at a rate of 0.52 ± 0.11 Pg carbon per year according to the models. This estimate is 28% ± 20% lower than that derived from observations. Further investigation reveals that about 70% of the accumulated anthropogenic carbon is taken up from the atmosphere, while the remainder is imported from the Southern Ocean.

1. Introduction

During the International Geophysical Year 1957–1958, Taro Takahashi (1930–2019) made the first systematic and accurate measurements of carbon dioxide gas (CO_2) partial pressure in the air and sea surface along an

Data curation: N. Goris, M. López-Mozos, J. D. Müller, I. E. Huertas, T. T. T. Chau, V. Cainzos, A. Velo, G. Benard, Rik Wanninkhof
Formal analysis: Fiz F. Pérez, M. Becker, N. Goris, M. Gehlen, J. Tjiputra
Investigation: Fiz F. Pérez, M. Becker, N. Goris, M. López-Mozos, J. Tjiputra, J. D. Müller, I. E. Huertas, T. T. T. Chau, V. Cainzos, A. Velo
Methodology: Fiz F. Pérez, M. Becker, N. Goris, J. Tjiputra, A. Olsen, J. D. Müller, Rik Wanninkhof
Project administration: J. D. Müller, Rik Wanninkhof
Resources: M. López-Mozos, A. Olsen, J. D. Müller, I. E. Huertas, Rik Wanninkhof
Software: M. Becker, N. Goris, M. López-Mozos, J. Tjiputra, J. D. Müller, I. E. Huertas, T. T. T. Chau, V. Cainzos, A. Velo, G. Benard, Rik Wanninkhof
Supervision: Fiz F. Pérez, N. Goris, M. Gehlen, J. Tjiputra, A. Olsen, J. D. Müller, J. Hauck, N. Gruber, Rik Wanninkhof
Validation: Fiz F. Pérez, J. Hauck, N. Gruber, Rik Wanninkhof
Visualization: M. Becker, N. Goris, M. López-Mozos, J. Tjiputra
Writing – original draft: Fiz F. Pérez, N. Goris, M. López-Mozos, J. Tjiputra, A. Olsen, J. D. Müller, I. E. Huertas
Writing – review & editing: Fiz F. Pérez, M. Becker, N. Goris, M. Gehlen, M. López-Mozos, J. Tjiputra, A. Olsen, J. D. Müller, I. E. Huertas, T. T. T. Chau, J. Hauck, N. Gruber, Rik Wanninkhof

Atlantic Ocean transect from Greenland to Cape Town (Takahashi, 1961). Since these early times, the importance of monitoring seawater CO_2 partial pressure (pCO_2) for the assessment of sea-air exchanges of CO_2 has been increasingly recognized. Today, measurements of pCO_2 have become an integral part of ocean monitoring programs including Eulerian time series stations (Bates et al., 2014), oceanographic buoy arrays, and Ships of Opportunity (SOOP) programs (Bakker et al., 2016; Pfeil et al., 2013; Sabine et al., 2013; Wanninkof et al., 2019). Early measurements of pCO_2 highlighted spatial patterns that were confirmed later by time-series measurements (Bates et al., 1998; Gruber et al., 1998; Keeling, 1993; Michaels et al., 1994), large-scale data compilations and the development of surface ocean CO_2 climatology (Takahashi et al., 2002, 2009). The North Atlantic between 25°N and 76°N stands out as a region of intense CO_2 uptake by the ocean. It represents only 7% of the ocean surface, but accounts for 23% of the global uptake (Schuster et al., 2013; Takahashi et al., 2009). Approximately two thirds of its contemporary uptake is caused by natural processes, such as heat loss and export production, while the remaining one third is caused by the increasing concentrations of CO_2 in the atmosphere and is therefore called uptake of anthropogenic carbon, C_{ant} (Gruber et al., 2009; Keeling & Peng, 1995; Mikaloff Fletcher et al., 2007; Watson et al., 1995). The local uptake of C_{ant} by sea-air exchange in the Atlantic combined with the net northward transport of C_{ant}-rich southern latitude waters by the upper limb of the Atlantic meridional overturning circulation (AMOC) (Brown et al., 2021; MacDonald et al., 2003; Pérez et al., 2013; Rosón et al., 2003) leads to a high accumulation of C_{ant} throughout the water column of the Atlantic, accounting for approximately 35% of the global total storage (Gruber et al., 2019; Sabine et al., 2004). Earlier studies highlighted the role of the AMOC, a key component of the global ocean circulation and a distinctive dynamic element of the Atlantic circulation, in the redistribution of CO_2 (Holfort et al., 1998; Wallace, 2001). The AMOC further links the upper ocean thermohaline circulation with the intense Deep Western Boundary Current (DWBC) connecting the waters formed in the subpolar North Atlantic with the Southern Ocean (Haine, 2016; Hirschi et al., 2020; Rhein et al., 2015). The DWBC contributes to natural interhemispheric carbon exchanges by transporting between 0.5 and 1 PgC yr^{-1} from North Atlantic uptake regions southward (Aumont et al., 2001; Macdonald et al., 2003; Resplandy et al., 2018).

As part of the second phase of the Regional Carbon Cycle Assessment and Processes project (RECCAP2), we complement these earlier studies about the Atlantic carbon budget with an analysis of the latest observation- and model-based estimates of the Atlantic Ocean including sea-air fluxes (natural and anthropogenic), storage, and transport of CO_2 for the years 1985–2018. Following Fay and McKinley (2014), RECCAP2 divides the Atlantic into five regions or biomes (Figure 1a), namely the North Atlantic subpolar gyre (NA SPSS), the seasonally and permanently stratified regions of the North Atlantic subtropical gyre (NA STSS and NA STPS), the Atlantic equatorial upwelling region (AEQU), and the permanently stratified South Atlantic subtropical gyre extending southward to ~35°S (SA STPS). The Mediterranean Sea is also included as a single, sixth biome (MED). Among these regions, the NA SPSS stands out as a biome with high spatial and temporal variability, which still challenges our understanding, assessments, and modeling efforts despite the increase in observational capacity over the last two decades. During the RECCAP1 period (1990–2009), Schuster et al. (2013) estimated an average CO_2 uptake of -0.21 ± 0.06 PgC yr^{-1} ***(positive sign indicating flux into the atmosphere (outgassing), and negative sign a flux into the ocean (uptake))*** between 49°N and 79°N, consistent across observation-based estimates and numerical models used. This flux amounts to 10% of the global uptake and makes the NA subpolar region one of the regions with the highest CO_2 uptake density (see Text S1 in Supporting Information S2). Understanding the seasonal, interannual and long-term variability of the high latitude Atlantic CO_2 sink has been the focus of many observational and modeling studies (e.g., Breeden & McKinley, 2016; Goris et al., 2015; Leseurre et al., 2020; Macovei et al., 2020; Thomas et al., 2008; Tjiputra et al., 2012; Ullman et al., 2009; Watson et al., 2009). It has become clear that the variability of sea-air fluxes of CO_2 and C_{ant} storage rates in this region is influenced by regional modes of climate variability, such as the North Atlantic Oscillation (NAO), through its effect on wind patterns and ocean heat loss, mixing, and deep water formation. During the time period from the 1990s to the 2000s, C_{ant} storage rates decreased in the subpolar NA in response to the shift from predominantly high (1990–1995) to low (2002–2007) NAO (Gruber et al., 2019; Pérez et al., 2008, 2013; Steinfeldt et al., 2009). As part of their global assessment, Müller et al. (2023) found that only the North Atlantic exhibited a trend toward weaker C_{ant} accumulation relative to the atmospheric CO_2 increase by comparing their inventory changes from 2004 to 2014 and from 1994 to 2004 with previous estimates for the period 1800 to 1994 from Sabine et al. (2004). However, recent observations show a reinvigoration of the C_{ant} accumulation at the local scale associated with increased convection in the mid 2010s (Fröb et al., 2016), as a consequence of a shift back to positive NAO conditions.

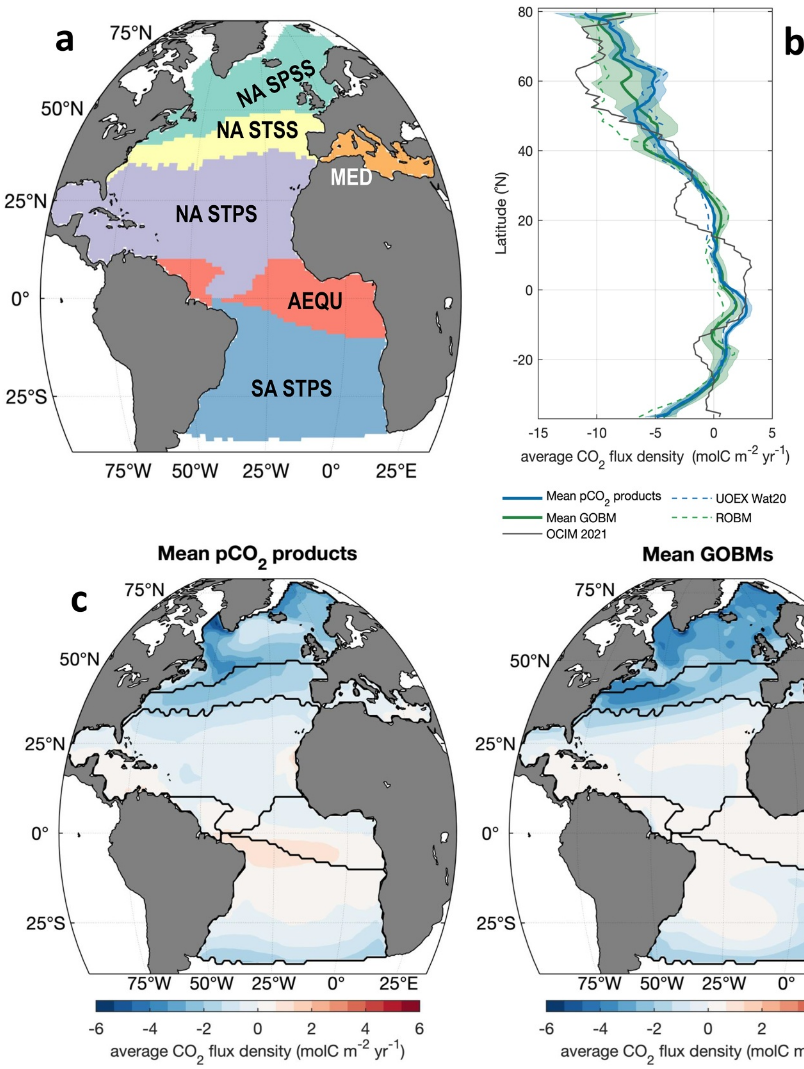

Figure 1. (a) RECCAP2 biomes in the Atlantic including the Mediterranean Sea. (b) Latitudinal variation of CO_2 flux densities displayed for the ensemble mean of the pCO_2 products, the GOBM ensemble mean, the UOEX data product that corrects for skin temperature effects, the regional hindcast model (ROBM), and the inverse model OCIMv2021. Average CO_2 flux density from 1985 to 2018, illustrated on maps for the ensemble means of (c) nine pCO_2 products and (d) 11 GOBMs. Negative values indicate oceanic uptake of CO_2. The biomes are the seasonally stratified North Atlantic subpolar gyre (NA SPSS), the seasonally and permanently stratified regions of the North Atlantic subtropical gyre (NA STSS and NA STPS), the Atlantic equatorial upwelling region (AEQU), the seasonally stratified South Atlantic subtropical gyre (SA STPS), and the Mediterranean Sea (MED). Note that the GOBMs do not adequately represent the RCO (Riverine CO_2 outgassing) fluxes and thus we did not adjust those with other available estimates.

The subtropical North Atlantic (in RECCAP1 defined to be 18° to 49°N, 7.2% of the ocean surface, see Text S1 in Supporting Information S2) was shown to be a CO_2 sink, with a net uptake of -0.26 ± 0.06 PgC yr^{-1} between 1990 and 2009 (Schuster et al., 2013), comprising approximately equal parts to C_{ant} and natural CO_2 uptake, where the latter is driven mainly by net heat loss, with limited contributions from biological activity (Gruber et al., 2009). The mean subtropical gyre uptake rate (-0.91 mol C m^{-2} yr^{-1}) is similar to that observed in the Bermuda Atlantic Time-series Study (Bates et al., 2014), even though the eastern return branch of the subtropical gyre showed lower uptake values (Santana-Casiano et al., 2009). At both sites, the interannual variability of CO_2 flux correlates with sea surface temperature (SST) and mixed layer depth anomalies (González-Dávila et al., 2010; Gruber et al., 2002; Santana-Casiano et al., 2009). SST is the main driver of the seasonal cycle in the subtropics, driving an outgassing of CO_2 in summer and uptake in winter.

The tropical Atlantic is the second largest oceanic source of CO_2 to the atmosphere, after the tropical Pacific, with an annual emission of 0.10–0.11 PgC yr^{-1} (Landschützer et al., 2014; Takahashi et al., 2009) due to frequent upwelling of cold, CO_2-rich water in the eastern parts. Based on six different methodologies, the RECCAP1 estimate for this region converged on an outgassing of 0.12 ± 0.04 PgC yr^{-1} between 1990 and 2009 (Schuster et al., 2013; see Text S1 in Supporting Information S2). The increase in atmospheric CO_2 has decreased the net outgassing since preindustrial times, as the ocean supersaturation is reduced by about 50% (Gruber et al., 2009). This implies an uptake of anthropogenic CO_2. Gruber et al. (2009) also suggested that an important part of this natural outgassing is due to the riverine contribution of organic matter, especially that stemming from the Amazon river (Louchard et al., 2021).

The subtropical South Atlantic is a sink for atmospheric CO_2 (Rödenbeck et al., 2015; Schuster et al., 2013), driven in almost equal parts by natural and anthropogenic CO_2 fluxes (Gruber et al., 2009). It has been suggested that strong upwelling events in the eastern part generate significant interannual variability (Schuster et al., 2013; see Text S1 in Supporting Information S2). However, pCO_2 variability in the SA STPS biome is relatively low, as shown by Rödenbeck et al. (2015). From 1990 to 2009, this region was a CO_2 sink of −0.14 ± 0.04 PgC yr^{-1} on average, combining areas with a net outgassing north of the 23°C isotherm (Ito et al., 2005) with areas of absorption to the south. This region is relatively poorly sampled, with the domain north of 31°S acting as a source in spring and sinking in autumn (González-Dávila et al., 2009; Padín et al., 2010; Santana-Casiano et al., 2007). Estimates of long-term CO_2 flux trends in this region are highly dependent on the methodology used (Schuster et al., 2013).

The Mediterranean Sea represents 3.5% of the Atlantic Ocean area and is the only mid-latitude ocean basin in which deep convection occurs (see Text S1 in Supporting Information S2). This circulation is responsible for a relatively large inventory of C_{ant} of 1.7 PgC in 2001 as estimated from CFCs (Schneider et al., 2010). The overturning time is fast in relation to that of the global ocean (60–220 years vs. more than 1,000 years; Khatiwala et al., 2013; Stöven & Tanhua, 2014) and allows a complete renewal of water in the basin on a centennial time scale. Hence, surface waters enriched in C_{ant} transfer this signature to deep layers relatively quickly, leading to all water masses in the basin being already invaded by C_{ant} (Hassoun et al., 2015; Touratier et al., 2016). However, surface pCO_2 exhibits large variability, due to the large heterogeneity of physical and trophic regimes in the two main Mediterranean sub-basins, with a marked west-to-east oligotrophy gradient and different atmospheric forcings that regulate seawater pCO_2 and the sea-air CO_2 exchanges (Coppola et al., 2018; De Carlo et al., 2013; Ingrosso et al., 2016; Kapsenberg et al., 2017; Krasakopoulos et al., 2009, 2017; Petihakis et al., 2018; Sisma-Ventura et al., 2017; Urbini et al., 2020; Wimart-Rousseau et al., 2021).

In RECCAP1, the assessment of the ocean carbon cycle relied on five global ocean biogeochemical models (GOBMs), several atmospheric and oceanic inversions, the pCO_2 climatology published by Takahashi et al. (2009), as well as the SOCAT (Surface Ocean CO_2 Atlas) database. A crucial progress since RECCAP1 is the annual update of SOCAT (Bakker et al., 2016), with over 33.7 million quality-controlled surface ocean pCO_2 measurements in the 2022 release (Bakker et al., 2022). The availability of these data sparked the development of time-varying reconstructions of surface ocean pCO_2 distributions. These pCO_2 products rely on advanced statistical techniques and neural networks to extrapolate sparse observations in time and space to achieve temporally resolved global coverage (e.g., Chau et al., 2022; Gregor et al., 2019; Landschützer et al., 2014; Rödenbeck et al., 2014). Similarly, advances in biogeochemical modeling since RECCAP1 led to the contribution of an increased number of GOBMs that provided output from up to four different simulations allowing to disentangle the natural carbon cycle and the anthropogenic perturbation (Friedlingstein et al., 2022; Wanninkhof et al., 2013).

Improved process understanding and increasing availability of ocean biogeochemical data have led to advances in GOBMs, particularly in simulating the large-scale features and mean state of the ocean carbon cycle (Séférian et al., 2020). When forced with atmospheric reanalysis and atmospheric CO_2 concentration data, these models were assessed to be suitable for quantifying the global ocean carbon fluxes, from annual mean to interannual time-scale (Hauck et al., 2020). Regionally, such models have also been shown to be capable of simulating the observed long-term pCO_2 trends (Tjiputra et al., 2014). Nevertheless, some GOBMs still have difficulties in representing the observed seasonal cycle in key ocean sink regions in the North Atlantic, likely owing to mismatch in the timing of deep winter mixing and/or biological bloom events (Schwinger et al., 2016; Tjiputra et al., 2012). Since RECCAP1, the number of GOBMs has increased from 6 to 11 in RECCAP2, and while not all RECCAP1 models participated in the RECCAP2 exercise, those that did have likely gone through iterations of improvements (the readers are referred to Table S1 in DeVries et al., 2023, for individual biogeochemical model descriptions). In the Atlantic domain, recent developments in the ocean physical component have led to better representation of large scale circulation and ventilation processes (Hirschi et al., 2020), which could have strong implications on the transports of biogeochemical tracers driving the sea-air CO_2 fluxes and interior carbon sequestration in this basin.

This synthesis paper is structured as follows. Section 2 provides the details of the database consisting of data sets based on observations of both surface pCO_2 and the marine carbonate system in the ocean interior, and an ensemble of global biogeochemical models together with a regional model and an assimilation model. In Section 3, the CO_2 fluxes obtained for each class of products are described and analyzed considering both the mean values for the study period, trends in two periods (1985–2000 and 2000–2018), the seasonal cycle and the interannual variability of CO_2 fluxes. In addition, the accumulation of anthropogenic CO_2 in the ocean interior is evaluated. In Section 4, we discuss the results obtained in RECCAP2 in comparison to RECCAP1, as well as the consistency and discrepancies between the global biogeochemical models and different data products, and suggest ways for future improvements. Section 5 summarizes the main conclusions and lists some of the remaining challenges to be solved in future versions of RECCAP.

2. Methods

The Atlantic Ocean and its subdivision into biomes is defined by the RECCAP2 basin mask (Müller, 2023) that builds on the biome definition by Fay and McKinley (2014) and extends from approximately 79°N to approximately 35°S (Figure 1). The RECCAP2 ocean database used in this study is described by DeVries et al. (2023), consisting of observation-based and model-based products. Here, we use two types of observation-based products, namely surface ocean pCO_2 (pCO_2 products) and ocean interior C_{ant} reconstructions. For model-based products, we use Global and Regional Ocean Biogeochemical Model (GOBM/ROBM) hindcast simulations and an ocean data-assimilation model. All products were re-gridded onto a common $1° \times 1°$ horizontal grid and monthly temporal resolution by the data providers, except for ocean interior model outputs, which were submitted as annual averages. Ocean model outputs were either provided on the models' standard depth levels or regridded to fixed depth levels chosen by the data providers.

2.1. Observation-Based Products

2.1.1. pCO_2 Products

This analysis draws on a variety of observation-based products for surface ocean pCO_2 and sea-air CO_2 fluxes (Table S1 in Supporting Information S2). These products are based on the interpolation of in situ pCO_2 data accessed from different releases (v2019-v2021, v5) of SOCAT (Bakker et al., 2016) to near-global coverage. Several interpolation methods are used including machine learning techniques (Chau et al., 2022; Gloege et al., 2021; Gregor & Gruber, 2021; Gregor et al., 2019; Iida et al., 2021; Landschützer et al., 2014; Watson et al., 2020; Zeng et al., 2022) and a diagnostic mixed layer scheme (Rödenbeck et al., 2013). Sea-air CO_2 fluxes (FCO_2) are computed from reconstructed pCO_2 fields following:

$$FCO_2 = Kw\left(1 - f_{ice}\right) K_0 \left(pCO_2 - pCO_2, air\right) \tag{1}$$

where Kw is gas transfer velocity; f_{ice} is sea-ice cover fraction; K_0 is CO_2 solubility in seawater; and pCO_2, and pCO_2, air are the partial pressures of CO_2 in seawater (nominally at 5 m depth) and in the overlying atmosphere, respectively. The gas transfer velocity is computed as a function of wind speed at 10 m, mostly assuming a quadratic relationship (Ho et al., 2006; Nightingale et al., 2000; Wanninkhof, 1992, 2014). For the set of pCO_2 products, the uncertainty of the mean is determined as the standard deviation of the FCO_2 of the nine pCO_2 products referenced in Table S1 of the Supporting Information S2.

The pCO_2 product by Watson et al. (2020), UOEX-Wat20, is different from the other products as it adjusts the underlying pCO_2 observations accounting for the cool-skin effect and for near-surface temperature gradients following Goddijn-Murphy et al. (2015) and Woolf et al. (2016), henceforth referred to as the surface skin effects. While it applies the SOMFFN interpolation approach also used in MPI-SOMFFN, it does so in different fashion such that the differences between the UOEX-Wat20 and other approaches are not solely attributed to adjusting the

pCO_2 values. While UOEX-Wat20 is included in the analysis, it is kept distinct from the other nine pCO_2 products, because of the difference in approach.

The pCO_2 products all use the bulk flux parameterization (Equation 1) and aside from UOEX-Wat20 follow the convention of reference depth for pCO_2 at nominally 5-m. The uncertainty estimates provided here are mainly based on differences between the different products. Uncertainties and biases in gas transfer velocities, and impacts of near- surface pCO_2 gradients (Bellenger et al., 2023; Dong et al., 2022) are not taken into account but are estimated to increase the uncertainty in the pCO_2 products by 3-fold on global scales (see Table 3, DeVries et al., 2023).

2.1.2. Ocean Interior C_{ant} Reconstructions

Furthermore, we consider two ocean interior observation-based products, one based on measurements of dissolved inorganic carbon (DIC) concentrations collected over more than 30 years, and other physical and biogeochemical parameters by Gruber et al. (2019), and another one combining an inversion approach with tracer measurements by Khatiwala et al. (2009). The Gruber et al. (2019) product provides an estimate of the ocean C_{ant} storage change (ΔC_{ant}) between the years 1994 and 2007. This estimate is based on the eMLR(C*) method (Clement & Gruber, 2018) applied to the GLODAPv2 data (Olsen et al., 2016). It includes estimates from surface to 3,000 m depth for both the steady-state and non-steady-state components of ΔC_{ant} in the ocean interior. In the North Atlantic and below 3,000 m, Gruber et al. (2019) estimated an inventory change C_{ant} of 0.05 PgC yr^{-1} (~8% of the accumulation above 3,000 m), which has been proportionally distributed across biomes according to the GOBM ΔC_{ant} below 3,000 m. The product from Khatiwala et al. (2009) provides estimates of the increase of the oceanic C_{ant} content from 1850 up to 2011 and is based on a Green's Function approach that allows a gradual increase in the CO_2 disequilibrium between the atmosphere and the ocean.

The C_{ant} reconstruction product from Khatiwala et al. (2009) was pre-processed to match the RECCAP2 $1° \times 1°$ grid and depth levels of the ΔC_{ant} reconstruction from Gruber et al. (2019). Since the product provides annual values, we calculated ΔC_{ant} between 1994 and 2007 to allow for comparison with Gruber et al. (2019). The ΔC_{ant} reconstruction of Gruber et al. (2019) does not cover the entire NA SPSS biome explored in our study, so we extrapolated the product to the Nordic Seas assuming the same vertical ΔC_{ant} profile as at 65°N, resulting in a 23% increase of ΔC_{ant} storage rate in the NA SPSS biome. The percentage of increase obtained was also applied to Khatiwala et al. (2009), as it also does not fully cover the NA SPSS biome. The uncertainty in the C_{ant} inventory increase in each biome was estimated by surface area scaling of the uncertainties of the North and South Atlantic provided by Gruber et al. (2019). For the Khatiwala et al. (2009) product, a relative uncertainty of 17% was set following Khatiwala et al. (2013).

2.2. Global Ocean Biogeochemical Models

As an improvement from RECCAP1 (Wanninkhof et al., 2013), the RECCAP2 protocol provides a set-up of four simulations with four combinations of atmospheric physical and CO_2 concentration forcings such that the simulated total CO_2-fluxes can be divided into their steady-state and non-steady state natural and anthropogenic components: (a) Simulation A: temporally varying atmospheric forcing and increasing atmospheric CO_2, (b) Simulation B: climatological atmospheric forcing and constant pre-industrial atmospheric CO_2, (c) Simulation C: climatological atmospheric forcing and increasing atmospheric CO_2, and (d) Simulation D: temporally varying atmospheric forcing and constant pre-industrial CO_2.

We used outputs from 11 GOBMs of which the majority also contributed to the Global Carbon Budget (Friedlingstein et al., 2022; Table S2 in Supporting Information S2). All GOBMs used here are general ocean circulation models with coupled ocean biogeochemistry, run in hindcast mode and hence forced by atmospheric data sets. Details of the respective model resolutions, forcings, and references are provided in an overview table in DeVries et al. (2023). All models performed four simulations (A, B, C, and D), except for MOM6-Princeton (not C and D). Additionally, we considered the output from the regional ocean biogeochemical model (ROBM) ROMS-AtlanticOcean-ETHZ (Louchard et al., 2021) that only performed Simulation A. We also included results from the ocean data-assimilation model OCIMv2021 (DeVries, 2022) that performed simulations A, B, and C. OCIMv2021 uses a climatological mean circulation but has a time-varying SST. It includes an abiotic carbon cycle model forced with atmospheric CO_2 to estimate the anthropogenic carbon distribution.

To determine the FCO_2 for the period 1985–2018, for each GOBM and each biome, we subtracted the linear trend of the respective fluxes estimated in Simulation B from Simulation A, to correct for potential model-dependent drift. For the ensemble of GOBMs, the uncertainty of the mean was determined as the standard deviation of the 11 models referenced in Table S2 of the Supporting Information S2.

In order to be consistent with the ΔC_{ant} reconstruction of Gruber et al. (2019), the C_{ant} accumulation rate in the GOBMs was evaluated between 1994 and 2007. Here, C_{ant} was calculated as the difference in DIC between the simulation with increasing atmospheric CO_2 concentrations (Simulation A) and the one with constant pre-industrial atmospheric CO_2 concentrations (Simulation D), both with time-varying atmospheric physical forcing. We considered all GOBMs that ran Simulation A and Simulation D (Table S2 in Supporting Information S2). However, MPIOM-HAMOCC was excluded from the final analysis because of its large negative C_{ant} values in the interior due to inconsistent physical forcing between its Simulations A and D. For the OCIMv2021 model, C_{ant} was determined as the difference between Simulations C (increasing atmospheric CO_2, climatological atmospheric forcing) and B (constant pre-industrial atmospheric CO_2, climatological atmospheric forcing), as this model uses a steady-state circulation and did not run Simulation D. Once we obtained the total C_{ant} concentrations from all GOBMs, we computed the C_{ant} storage changes as the difference between the concentrations in 1994 and 2007. C_{ant} concentration changes were vertically integrated to get the column inventory storage changes, as well as biome-integrated ΔC_{ant} rates. For the GOBM ensemble, the uncertainty of the mean ΔC_{ant} rate is determined as the standard deviation of the ΔC_{ant} rates of the nine models referenced in Table S2 of the Supporting Information S2.

2.3. Area Coverage

Practically all pCO_2 products considered have a spatial coverage of almost 100% of the Atlantic basin, except JMA-MLR and MPI-SOMFFN with about 91%–92% of the area coverage in the northernmost biome (NA SPSS). Here, pCO_2 product fluxes were not scaled to the same ocean area, following the assumption of Hauck, Gregor, et al. (2023), that the discrepancy arising from differences in covered area are smaller than the uncertainty arising from any extrapolation to an equal area. All GOBMs cover more than 98% of the area, except MPIOM-HAMOCC (95%) and CESM-ETHZ (97%). ROMS-ETHZ (ROBM) covers 95% of the Atlantic Region, and only 93% of the NA SPSS biome and 25% of the Mediterranean Sea. Likewise, most of the missing coverage of the MPIOM-HAMOCC is located in the Mediterranean Sea, thus ROMS-ETHZ and MPIOM-HAMOCC have not been used for the evaluation of the MED biome.

2.4. Riverine Carbon Outgassing

The flux of natural CO_2 across the sea-air interface also includes a flux balancing the input of inorganic and organic carbon at the land-sea interface minus the fraction buried in marine sediments (Regnier et al., 2013; Sarmiento & Sundquist, 1992). We refer to this flux component as preindustrial riverine CO_2 outgassing (RCO). Since pCO_2 products are based on real-world observations, they provide estimates of total FCO_2, including the RCO. In contrast, RCO is not at all or not adequately represented in GOBMs. Its approximation would require several thousands of years of integration with a GOBM including a sediment module. None of the GOBMs used here includes such a long pre-industrial spin-up (Terhaar et al., 2024). Though several of the GOBMs analyzed in this study include river inputs of carbon, not all processes relevant for the land-sea flux are adequately represented. In consequence, the average of the global imbalance between river input and flux to the sediment is small (<0.14 PgC yr^{-1}) in the GOBM ensemble (Terhaar et al., 2024) compared to the observation-based global integral of RCO recommended in the RECCAP2 protocol, that amounts to 0.65 ± 0.3 PgC yr^{-1} (Regnier et al., 2022). Combining the spatial distribution of RCO by Lacroix et al. (2020) and the globally integrated estimate by Regnier et al. (2022) allows us, in principle, to estimate its contribution to FCO_2 at biome scale, albeit with a relative uncertainty that is most likely even larger than that of the global integral (>50% of the absolute value) and without considering the already-present land-sea fluxes of the GOBMs. However, the magnitude of RCO is a major source of uncertainty and hinders the straightforward comparison of fluxes from pCO_2 products and GOBMs. In our analysis, we chose not to add the estimated RCO to the GOBMs but to present it separately, whenever this is meaningful. As the RCO spatial distribution by Lacroix et al. (2020) is uncertain, we do not evaluate it on a grid scale but only at the biome scale.

3. Results

3.1. Sea-Air CO_2 Fluxes

3.1.1. Long-Term Mean Fluxes From 1985 to 2018: Spatial Patterns and Regional Integrals

The mean sea-air CO_2 fluxes of the pCO_2 products and GOBMs have very similar spatial patterns when averaged over the 1985 to 2018 period (Figures 1c and 1d). The pCO_2 products show a weak CO_2 outgassing over large areas of the tropical regions of the South and North Atlantic, which is more intense in the western equatorial Atlantic. In comparison, the GOBMs exhibit weaker CO_2 fluxes in the equatorial region but more intense CO_2 fluxes in the Benguela and Mauritanian upwelling areas. In these upwelling regions, the ocean circulation delivers nutrients and DIC to the surface layer where they are consumed by photosynthesizing organisms. In many of these regions, the supply of DIC from below exceeds the amount of DIC being drawn down by the net balance between photosynthesis and remineralization/respiration, that is, net community production, such that an excess of DIC and nutrients remain at the surface, indicative of an inefficient biological pump (Sarmiento & Gruber, 2006). As a result, these regions act as a source of CO_2 to the atmosphere. Downstream of many of these regions, the remaining nutrients and the DIC get drawn down completely. This resulting large increase in the biological pump efficiency makes these regions strong uptake regions. The NA SPSS and NA STSS biomes, and the southern parts of biome SA STPS are characterized by strong CO_2 uptake with some differences between the spatial patterns modeled in the GOBMs and those derived from observations. In these regions, both the cooling of the warm poleward moving waters and an efficient and strong biological pump promote CO_2 uptake from the atmosphere (Takahashi et al., 2009; Thomas et al., 2008; Watson et al., 1995).

pCO_2 products and GOBMs are in good agreement with respect to their zonally integrated CO_2 fluxes when regarding the northern hemisphere between equator and 40°N and the southern hemisphere south of 20°S (Figure 1b). The GOBMs show a more intense ocean uptake of CO_2, coinciding with the deep convection regions in the subpolar gyre (NA SPSS biome). In this region, models underestimate the transport and mixing of high subsurface DIC water to the surface during winter, underestimating the winter-time outgassing from the ocean (McKinley et al., 2018). The results obtained with the ROBM are very similar to that of the GOBMs between 35°S and 52°N, while the ROBM seems to overestimate uptake north of 52°N even more than the GOBMs. The inverse model OCIMv2021 follows the large-scale pattern of the other products, but shows more meridional variations and, similar to the ROBM, it also simulates a much stronger uptake than seen in models and observations north of 52°N (Figure 1b).

As shown in Figure S1 of the Supporting Information S1, the SOCAT gridded data of pCO_2 covers the NA SPSS biome with the highest number of observations among the Atlantic biomes, resulting in an average of 10.2% of the maximum possible coverage since 2003 and making it one of the regions where the pCO_2 products are expected to provide comparatively robust results. The UOEX data product, that adjusts the pCO_2 for near-surface temperature and salinity gradients, shows higher CO_2 uptake than the ensemble mean of the other pCO_2 products between 35°S and 50°N. This difference contains the expected effect of lower skin temperature on solubility, for which adjustments have been made in the UOEX product, but it also inherits the influence of different gap filling methods. Dong et al. (2022) have globally reevaluated the effect of skin temperature on FCO_2, showing an impact on FCO_2 that is 30% lower than that previously evaluated by Watson et al. (2020). The net effect of skin SST and salinity on FCO_2 integrated over the whole Atlantic and its five biomes is detailed in Table S4 of the Supporting Information S2. The change in CO_2 uptake due to the temperature effects estimated by Dong et al. (2022) is overall similar to the difference in FCO_2 between UOEX and the ensemble mean of nine pCO_2 products except for NA SPSS and SA STPS, where the different gap-filling methodology has a greater effect.

Integrated over the whole Atlantic Ocean, the average sea-air CO_2 flux (FCO_2) for the period 1985 to 2018 obtained from the GOBMs (**−0.47 ± 0.15** PgC yr^{-1}) is higher than that obtained from the pCO_2 products (**−0.36 ± 0.06** PgC yr^{-1}; Figure 2), although the difference is within the FCO_2 variability across the 11 GOBMs. OCIMv2021 estimates a larger uptake (−0.58 ± 0.08 PgC yr^{-1}) than the GOBMs. The ROBM simulates an uptake of −0.61 ± 0.14 PgC yr^{-1}, about 30% and 65% stronger than the mean of the GOBMs and pCO_2 products, respectively. Relative to the mean of the pCO_2 products, the CO_2 uptake in UOEX is larger by about 23%.

The NA SPSS biome, which covers only 15% of the Atlantic Ocean surface area, has the largest CO_2 uptake and also the largest differences between models and observational products (Figures 1 and 2, Table 1). Here, the mean FCO_2 of the GOBMs, the ROBM and OCIMv2021 indicate 26%, 59%, and 64% greater carbon uptake,

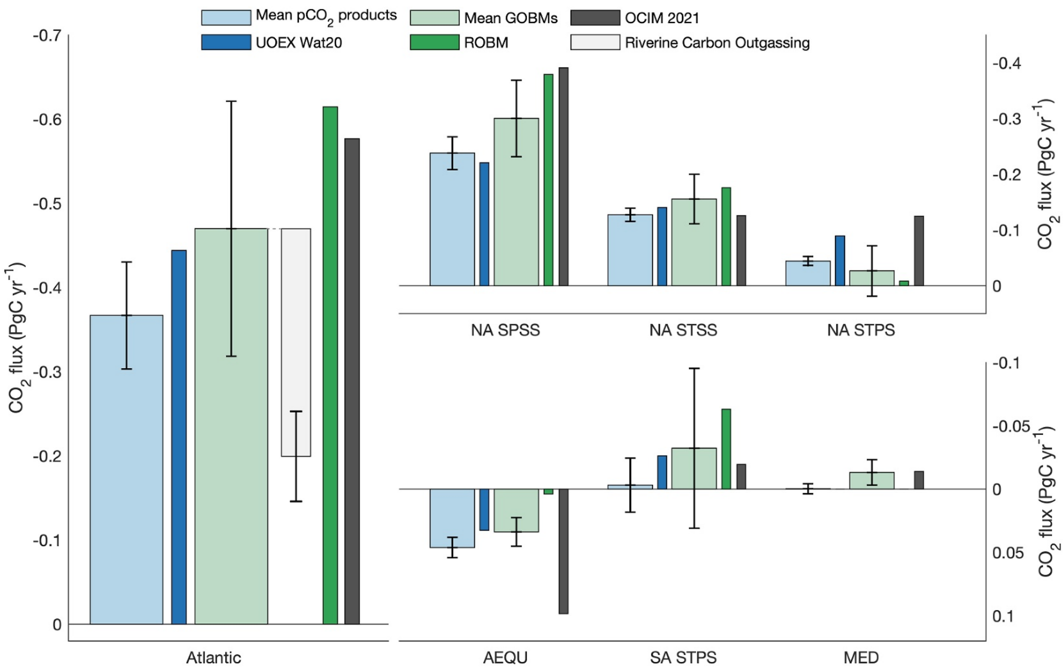

Figure 2. Spatially integrated sea-air CO_2 fluxes from 1985 to 2018 for the Atlantic and each Atlantic biome as estimated by nine pCO_2 products, 10 GOBMs, the UOEX pCO_2-data product, the ROBM and OCIMv2021. The white bar indicates an estimate for the outgassing of riverine carbon integrated over the whole Atlantic region, which is a flux component captured by the pCO_2 products but not by the GOBMs or the ROBM. Whiskers stand for standard deviation around the mean of the estimates. Negative values indicate the uptake of CO_2 from the atmosphere. Note that the *y*-axis are reversed, so that uptake is above the zero-line and outgassing is below it.

respectively, than the pCO_2 products. The spread between GOBMs is three times larger than it is for the pCO_2 products (Table S4 in Supporting Information S2). The uptake flux in UOEX is slightly lower (~7%) relative to the mean of pCO_2 products.

In the NA STSS biome, there is good agreement between the different pCO_2 products, with a standard deviation that is less than 10% of the mean (-0.13 ± 0.01 PgC yr^{-1}). Here, the UOEX product has 10% larger CO_2 uptake. With an average FCO_2 of -0.15 ± 0.04 PgC yr^{-1}, the GOBMs vary substantially more among each other, that is, ±30%. In fact, one GOBM has a ~50% weaker uptake than the GOBMs mean, while the GOBMs with the most intense fluxes are only 20% above the GOBMs mean. OCIMv2021 simulates FCO_2 values of similar magnitude to the pCO_2 products (Table S4 in Supporting Information S2).

For the NA STPS biome, pCO_2 products estimate a mean CO_2 uptake of -0.044 ± 0.008 PgC yr^{-1} with a very high homogeneity in spite of the large area of this biome. In comparison to the pCO_2 products, the uptake simulated by the GOBMs is smaller (-0.020 ± 0.040 PgC yr^{-1}), and with larger intermodel variations. Only three GOBMs estimated a CO_2 outgassing in this biome. In contrast, OCIMv2021 reported a quite high uptake of CO_2, almost three times larger than that of the pCO_2 products. The ROBM simulates a near-zero net flux in this biome. In the UOEX product, the uptake was twice as large as the mean of the other pCO_2 products.

All models and pCO_2 products agree that the AEQU biome is a net source of CO_2 to the atmosphere, consistent with the known impact of the equatorial upwelling that brings water with high DIC content to the ocean surface. The mean flux of the pCO_2 products is 0.046 ± 0.009 PgC yr^{-1}. In the UOEX product, this outgassing is 25% lower. The mean flux in the GOBMs is 0.035 ± 0.011 PgC yr^{-1}, and has relatively small inter-model variations. The ROBM simulates a very low outgassing. OCIMv2021 shows strong FCO_2, with more than double the outgassing of the mean GOBMs.

The SA STPS biome covers a large area, extending from the southern border of the equatorial region in the north toward the subtropical front of the Southern Ocean to the south. According to the mean of the pCO_2 products, the integrated flux over this region is neither a sink nor a source of CO_2 to the atmosphere (-0.003 ± 0.023 PgC yr^{-1}).

Table 1
Sea-Air Surface CO_2 Fluxes (1985–2018) and Anthropogenic CO_2 Accumulation Rates (1994–2007) of All Products Used in This Study, With Their Respective Standard Deviations or Uncertainties of Individual Estimates

Period	BIOME (Area · 10^{12} m^2)	FCO_2 ($PgC\ yr^{-1}$)			
		pCO2 products Ensemble mean	GOBM Ensemble mean	ROBM ROMS-ETHZ	Assimilation model OCIMv2021
1985–2018	**ATLANTIC** (68.7)	−0.37 ± 0.06	−0.47 ± 0.15	−0.61 ± 0.15	−0.58 ± 0.08
	NA SPSS (9.37)	−0.24 ± 0.03	−0.30 ± 0.07	−0.38 ± 0.05	−0.40 ± 0.03
	NA STSS (6.14)	−0.127 ± 0.012	−0.149 ± 0.041	−0.176 ± 0.022	−0.126 ± 0.012
	NA STPS (22.7)	−0.044 ± 0.008	−0.020 ± 0.041	−0.008 ± 0.026	−0.125 ± 0.024
	AEQU (8.69)	0.046 ± 0.008	0.035 ± 0.011	0.004 ± 0.016	0.098 ± 0.005
	SA STPS (19.6)	−0.003 ± 0.021	−0.029 ± 0.065	−0.063 ± 0.040	−0.020 ± 0.022
	MED (2.26)	0.000 ± 0.005	−0.015 ± 0.009	–	−0.014 ± 0.003
		ΔC_{ant} ($PgC\ yr^{-1}$)			
Period	BIOME (Area · 10^{12} m^2)	C_{ant} reconstruction Gruber et al., 2019	C_{ant} reconstruction Khatiwala et al., 2009	GOBM Ensemble mean	Assimilation model OCIMv2021
1994–2007	**ATLANTIC** (68.7)	0.72 ± 0.08	0.63 ± 0.11	0.52 ± 0.11	0.68 ± 0.01
	NA SPSS (9.37)	0.087 ± 0.007	0.149 ± 0.027	0.087 ± 0.033	0.127 ± 0.001
	NA STSS (6.14)	0.098 ± 0.005	0.105 ± 0.018	0.080 ± 0.031	0.107 ± 0.001
	NA STPS (22.7)	0.254 ± 0.017	0.199 ± 0.036	0.175 ± 0.045	0.236 ± 0.002
	AEQU (8.69)	0.058 ± 0.018	0.040 ± 0.007	0.037 ± 0.006	0.054 ± 0.001
	SA STPS (19.6)	0.216 ± 0.041	0.137 ± 0.025	0.127 ± 0.018	0.156 ± 0.001
	MED (2.26)	–	–	0.0176 ± 0.0068	0.0186 ± 0.0001

Note. For ΔC_{ant} the MED biome is not included in the total Atlantic estimate to facilitate direct comparison with Gruber et al. (2019). In each biome, the graduate yellow color background sorts the estimates from lowest flux into the ocean (light yellow) to largest flux into the ocean (dark yellow), as well as the estimates from lowest ΔC_{ant} (light yellow) to largest ΔC_{ant} (dark yellow).

But, the spread across the pCO_2 products is relatively large in this region, second only to the spread in the NA SPSS, in part because of the large area of the SA STPS biome. On average, the GOBMs indicate that this region is a CO_2 sink with an estimated integrated flux of −0.029 ± 0.076 $PgC\ yr^{-1}$. However, an integrated outgassing is simulated by 1/3 of the GOBMs. The FCO_2 in the ROBM is nearly twice as large as the mean of the GOBMs, while the OCIMv2021 suggested that the region behaves as a weaker CO_2 sink.

In the Mediterranean Sea, only five of the nine pCO_2 products have a regional coverage better than 95%. Of these, four pCO_2 products agree that the biome does not present significant sea-air CO_2 fluxes (Figure 2; Table S4 in Supporting Information S2). Most of the GOBMs have a coverage better than 95% and they broadly agree that the Mediterranean Sea represents a very weak CO_2 sink (−0.015 ± 0.010 $PgC\ yr^{-1}$). The flux in the OCIMv2021 is very similar. The ROBM has insufficient regional coverage for an assessment in this biome.

In summary, for the Atlantic, the GOBMs predict a 28% ± 14% larger CO_2 uptake than pCO_2 products (Table 1). The regional and data-assimilation models simulate a stronger Atlantic CO_2 sink than pCO_2 products by 67% and 57%, respectively (Table S4 in Supporting Information S2). The same is the case for the UOEX product, where the CO_2 uptake is 25% larger than that of the mean pCO_2 products, as a consequence of its adjustment for near surface temperature gradients.

3.1.2. FCO_2 Trends

The temporal evolution of the annual mean sea air fluxes in the pCO_2 products shows a change of rate around the year 2000 (Figure 3). In agreement with the recommended core analysis in RECCAP2, we thus analyzed changes in FCO_2 during two periods: between 1985 and 2000, and between 2001 and 2018. Over these two periods, the atmospheric CO_2 concentration increased on average by 1.5 and 2.1 ppm yr^{-1}, respectively, representing an acceleration in the atmospheric growth rate of 43% from the first to the second period. Integrated over the Atlantic

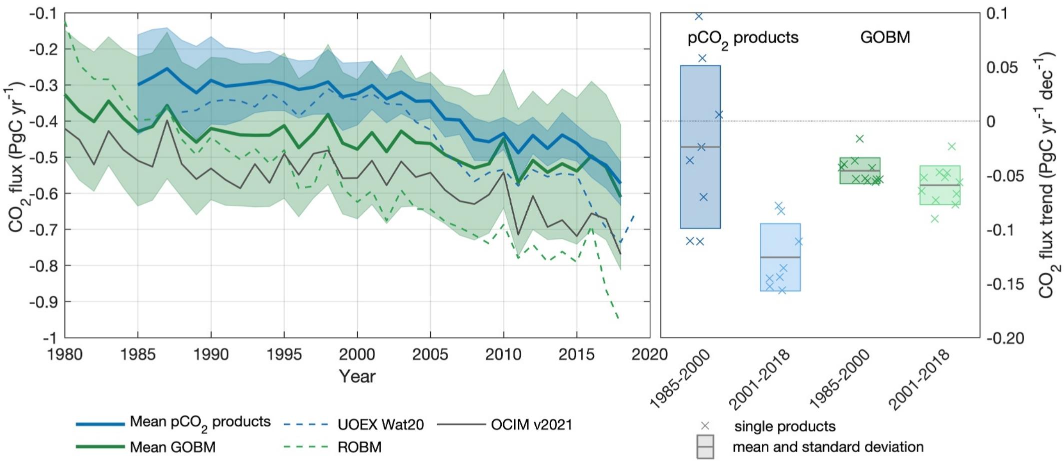

Figure 3. Trends in the sea-air CO_2-fluxes of the Atlantic Ocean. Time-series of the annual mean sea-air CO_2 fluxes (PgC yr^{-1}). Boxplots of the ensemble mean trends in sea-air CO_2 fluxes (PgC yr^{-1} dec^{-1}) and their 1σ spread before and after 2000. Shown are the ensemble of the pCO_2 products (blue) and GOBMs (green) on both panels, and UOEX, OCIM and one ROBM on the left panel.

as a whole, the pCO_2 products indicate a 5-fold increase in the growth rate of the ocean carbon sink from -0.024 ± 0.075 PgC yr^{-1} dec^{-1} between 1985 and 2000 to -0.126 ± 0.031 PgC yr^{-1} dec^{-1} between 2001 and 2018 (Figure 3). In contrast, GOBMs simulate only a 33% increase in the growth rate between the two periods, that is, from -0.045 ± 0.012 PgC yr^{-1} dec^{-1} between 1985 and 2000 to -0.060 ± 0.017 PgC yr^{-1} dec^{-1} between 2001 and 2018 (Figure 3). This is only slightly below the observed acceleration in the atmospheric CO_2 growth rate. The two products also differ strongly with regard to their spreads (Figure 3b). While the pCO_2 products exhibit a relatively low spread for the 1985–2018 mean flux, they differ considerably with regard to their FCO_2 trends. Conversely, GOBMs show a large spread in the 1985–2018 mean flux, but have a low spread in their FCO_2 trends in both periods, reflecting that the trends in the GOBMs are more strongly governed by the rate of change in atmospheric CO_2.

The CO_2 uptake trend increased in OCIMv2021 from -0.045 ± 0.016 PgC yr^{-1} dec^{-1} during the first period to -0.111 ± 0.018 PgC yr^{-1} dec^{-1} for the second period. Its estimate is thus similar to that of the GOBMs in the first period but almost twice as large in the second. The ROBM simulates a much stronger growth than the GOBMs in both periods (-0.19 ± 0.02 and -0.14 ± 0.02 PgC yr^{-1} dec^{-1}), but no significant change in trend. On the other hand, the UOEX pCO_2 product reveals an even greater contrast between the growth rates before 2000 (0.048 ± 0.014 PgC yr^{-1} dec^{-1}) and after 2000 (-0.188 ± 0.012 PgC yr^{-1} dec^{-1}) than the ensemble mean of the pCO_2 products. The trends obtained by the UOEX product showed a weakening of CO_2 uptake in the Atlantic Ocean before 2000, and an increase of about 0.35 PgC yr^{-1} in the second period, which is higher than in any of the other eight pCO_2 products (range: 0.14 to 0.28 PgC yr^{-1}). Three of the other pCO_2 products also suggest a weakening of the CO_2 uptake in the Atlantic before 2000, while four other products suggest increasing trends in CO_2 uptake by the Atlantic. Possibly the sharp contrast in observational coverage before and after the year 2000 (Figure S1 in Supporting Information S1; Bakker et al., 2022), as well as the availability of observed predictor data affected in a noticeable way some of the products. Indeed, the agreement among pCO_2 products significantly improved throughout the 1985–2000 period. This underscores a notable distinction from the GOBMs, as the observation-based trends in the initial period are markedly influenced by early-year FCO_2 estimates (Figure S2 in Supporting Information S1). During this period, only limited pCO_2 observations and predictor variables are available, and most products rely on climatology of specific predictors, such as chlorophyll and mixed layer depth, due to a scarcity of observational data.

Temporal trends in the individual biomes of the Atlantic are variable and highly dependent on the products used to estimate them (see Figure 4; Table S5 in Supporting Information S2). Between 2001 and 2018, the pCO_2 products show that the CO_2 uptake rate grows with values close to -0.03 PgC yr^{-1} dec^{-1} in the NA SPSS, NA STSS, NA STPS, and SA STPS biomes (which present very different areas) and -0.01 PgC yr^{-1} dec^{-1} in the AEQU biome. During this period, all pCO_2 products agreed on the sign of the trend in all biomes, with the exception of the MED

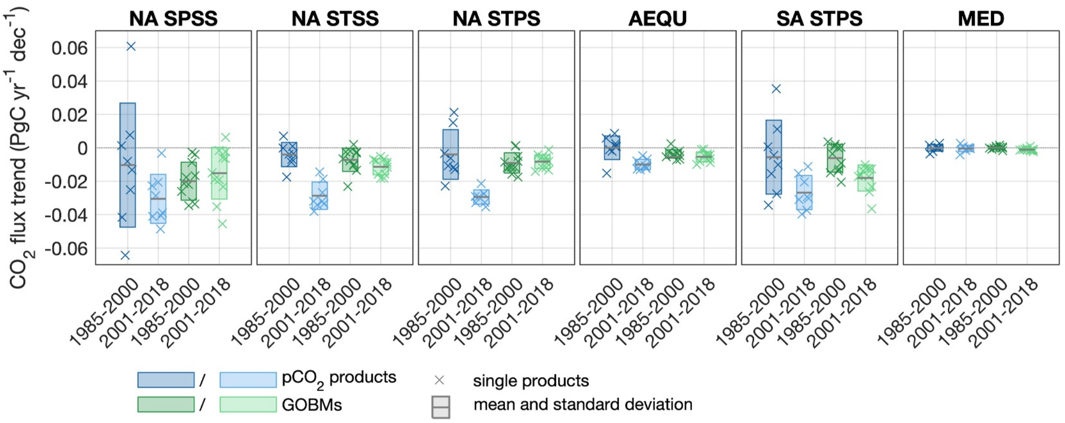

Figure 4. Trends in sea-air CO_2-fluxes for each Atlantic biome and two different time-periods as estimated by pCO_2 products (blue) and GOBMs (green). Shown are individual products (crosses), together with the ensemble mean and 1σ spread.

biome where the trend was consistently close to zero. However, for the period 1985–2000, trends in CO_2 uptake estimated by the pCO_2 products are more variable across the different products and biomes, with non-significant trends in FCO_2 in NA STPS (-0.004 ± 0.015 PgC yr^{-1} dec^{-1}), AEQU (0.000 ± 0.001 PgC yr^{-1} dec^{-1}), and SA STPS (-0.006 ± 0.022 PgC yr^{-1} dec^{-1}) and mark a notable contrast between the two periods.

The biome-level trends are more consistent across the GOBMs than across the pCO_2 products, and also more similar in the two periods. In three biomes, NA STSS, AEQU and SA STPS, the GOBMs simulate on average an increase in fluxes to the ocean between the first and the second periods. The disagreement among the GOBMs and between GOBMs and pCO_2 products is largest in the NA SPSS biome. The ROBM shows rates of increase of CO_2 uptake higher than -0.03 PgC yr^{-1} dec^{-1} in practically all biomes and in both periods except in NA STPS in the second one, and AEQU biomes in both (see Table S5 in Supporting Information S2). OCIMv2021 shows similar rates of increase to those observed in pCO_2 products for the second period, in line with the ROBM (Table S5 in Supporting Information S2).

3.1.3. Seasonal Cycle

The Atlantic Ocean sea-air CO_2 flux varies seasonally in a pronounced manner in all biomes, except for the equatorial (Figure 5). The Mediterranean Sea and the subtropical biomes (in their respective hemispheres) are CO_2 sinks in winter and sources in summer. Here, the impact of biological DIC drawdown on pCO_2 is relatively weak and seasonal warming and cooling dominate the seasonal cycle such that it peaks and reaches supersaturation in summer while minimum and undersaturated values occur in winter (Figures S3 and S4 in Supporting Information S1; Rodgers et al., 2023). The seasonal amplitude in the flux in these regions is slightly larger in the GOBMs than in the pCO_2 products. This has been attributed to a likely underestimation of seasonal mixed layer depth changes and seasonal drawdown of DIC by net primary production, such that the thermal component on the seasonal pCO_2 and sea-air CO_2 flux cycle is too strong in these models (Rodgers et al., 2023). The OCIMv2021 is an abiotic model and shows the largest seasonal pCO_2 (Figure S3 in Supporting Information S1) and flux variations because of the complete absence of biological processes. The difference in the seasonal cycle as modeled by the OCIMv2021 and the other GOBMs can be taken as a rough estimate of the importance of biology.

In the NA SPSS biome, the GOBMs' seasonal CO_2 flux cycle is similar to that in the subtropical biomes (and of the abiotic OCIM model), while that of the pCO_2 products is broadly reversed, apart from the summertime intermediate minimum in CO_2 uptake (Figure 5). The pCO_2 products have the highest pCO_2 values in winter, as a consequence of the supply of remineralized DIC into the surface layer through deep mixing (Figure S3 in Supporting Information S1). Seasonal stratification and increased light availability trigger spring blooms that cause a sharp pCO_2 decrease from March to June, after which the pCO_2 steadily increases back to its winter maximum. The existence of these patterns is well known from the many direct observations in this region (Becker et al., 2018; Fröb et al., 2019; Olsen et al., 2008; Takahashi et al., 1993). The opposite seasonal pCO_2 cycle in the GOBMs is likely due to the fact that their seasonal variations in mixed layer depths are too small (Rodgers et al., 2023), such that too few nutrients are upwelled during winter, likely resulting in an underestimation of

10.1029/2023GB007862

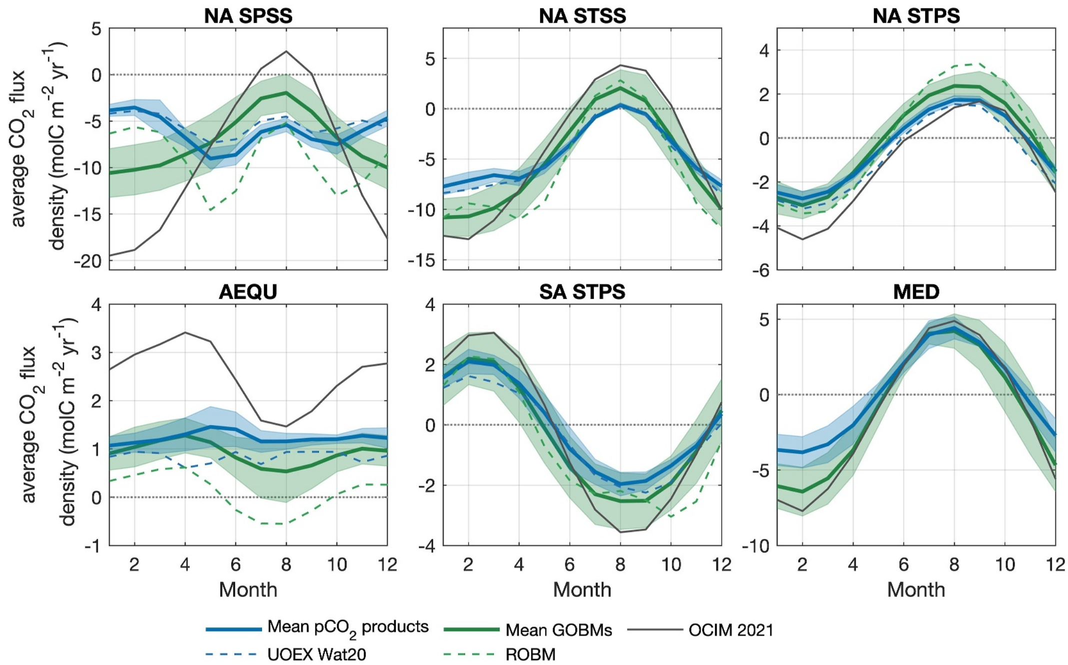

Figure 5. Seasonal cycle of the sea-air CO_2-fluxes for each Atlantic biome as estimated by pCO_2 products (blue) and GOBMs (green), both shown as the ensemble mean (thick lines) and 1σ spread (shadings) (1985–2018 average). Additional lines represent UOEX, OCIM and one ROBM. OCIM is an abiotic model and thus does not include the effect of the seasonality of net community production.

summer biological drawdown of DIC in the GOBMs (Rodgers et al., 2023; also shown for Earth System Models in Goris et al. (2018)). Since the opposing seasonal cycle of the GOBMs leads to a lower pCO_2 at the time of the strongest wind speeds, the GOBM ensemble shows higher annual net NA SPSS CO_2 uptake (Figures 1 and 2), that is, the GOBMs tend to simulate too strong uptake. Again, the OCIMv2021, as an abiotic model, is an extreme example of these model-effects. The ROBM appears more consistent with the pCO_2 products in this regard, but it overall appears to overestimate the NA SPSS CO_2 uptake as the modeled pCO_2 values are too low (Figure S3 in Supporting Information S1). The summertime intermediate minimum in CO_2 uptake in the pCO_2 products is a consequence of the minimum in wind speeds in that season. More quantitative analyses of the seasonal cycle including their drivers and differences between GOBMs and pCO_2 products are presented by Rodgers et al. (2023).

3.1.4. Interannual Variability of the Sea-Air CO_2 Fluxes

We further analyzed the interannual variability (IAV) of sea-air CO_2 fluxes, determined as the annual anomaly of the detrended sea-air CO_2 fluxes with respect to their mean values. Here, the removed linear trends and means are considered over the period 1985–2018 for pCO_2 products and GOBMs. When referencing the amplitude of IAV, we refer to the standard deviation of the so-derived detrended sea-air CO_2 flux anomalies. We find that, over the whole Atlantic basin, the IAV time-series of the sea-air CO_2 fluxes of GOBMs and pCO_2 products correlate relatively well (Figure 6d). Furthermore, both pCO_2 products and GOBMs show a high IAV amplitude in the northern parts and low IAV amplitude in the equatorial region (Figures 6a and 6b). This general spatial pattern of the IAV amplitude of net sea-air CO_2 fluxes has also been found in other studies (Brady et al., 2019; Park et al., 2010). However, the GOBMs show a larger IAV amplitude than the pCO_2 products in the interior subpolar gyre as well as in the eastern boundary upwelling regions (Figures 6a and 6b), while showing a smaller IAV amplitude for the NA SPSS biome as a whole (Figure 6e).

The pCO_2 products and GOBMs agree on the phasing of the IAV in net sea-air CO_2 fluxes, apart from in the subpolar region where correlations are small and negative (Figures 6c and 6e; Figure S5 in Supporting Information S1). We note that there is also little agreement in the IAV of this biome between pCO_2 products (Figure S6 in Supporting Information S1), while the GOBMs agree relatively well (Figure S6 in Supporting Information S1).

10.1029/2023GB007862

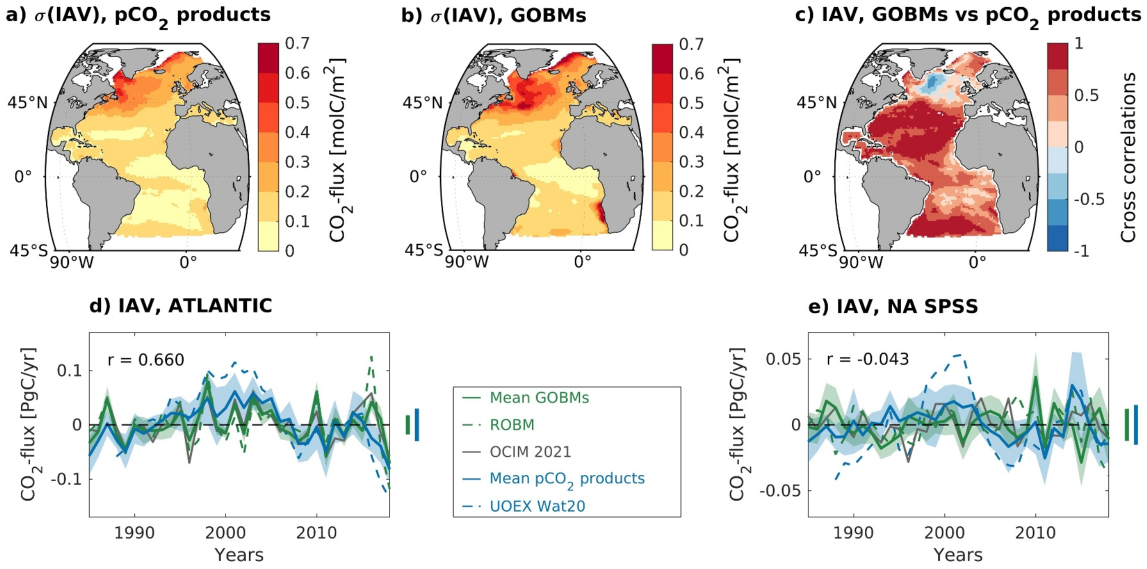

Figure 6. Interannual Variability (IAV) of observation-based and simulated sea-air CO_2 fluxes in the Atlantic. Panels (a and b) show the spatial distribution of the amplitude of IAV (calculated as standard deviation of the time-series of detrended annual sea-air CO_2 flux anomalies per grid point) for both (a) pCO_2 products and (b) GOBMs. Correlations between time-series of ensemble-averaged detrended sea-air CO_2 flux anomalies of GOBMs and pCO_2 products are shown in panel (c). Time-series of detrended annual sea-air CO_2 flux anomalies for both GOBMs (mean: green line; std: green shading) and pCO_2 products (mean: blue line; std: blue shading) are illustrated in panel (d) for the whole Atlantic and (e) for the NA SPSS biome, including the correlation coefficients between the time-series of GOBMs and pCO_2 products (denoted in the upper left corner of each panel d and e) and the amplitude of the IAV (illustrated as colored lines on the right side of each plot d and e).

GOBMs and pCO_2 products agree that the total sea-air CO_2 fluxes of the biomes NA STSS, NA STPS, and SA STPS are characterized by a moderate IAV amplitude (Figure S7 in Supporting Information S1), and that biomes AEQU and MED have only a weak IAV amplitude (see Figure S5 in Supporting Information S1). For these five biomes, GOBMs and pCO_2 products correlate reasonably well with respect to the temporal variability of the IAV with correlation coefficients ranging from $r = 0.57$ to $r = 0.73$ (see also Figure S5 in Supporting Information S1).

For the GOBM ensemble, the IAV of net sea-air CO_2 fluxes is strongly positively correlated to the IAV in SST (higher FCO_2 in anomalously warm years) over large parts of the Atlantic basin, most notably for both permanently stratified biomes (SA STPS and NA STPS) and the northwestern subpolar gyre (Figure S8b in Supporting Information S1). Along the Gulf Stream and the North Atlantic Current as well as regions of equatorial upwelling, the IAV in net sea-air CO_2 fluxes of the GOBM ensemble is weakly negatively correlated to the IAV in SST (higher FCO_2 in anomalously cold years). Due to the known dynamics of net sea-air CO_2 fluxes, these negative correlations imply that SST-variations are not the main driver of the IAV in net sea-air CO_2 fluxes but that the anomalous cold years are likely accompanied by stronger mixing and hence more DIC upwelling. As the thermodynamic boundary conditions used to force the GOBMs result in SSTs that have relatively strong fidelity to observations when averaged over biome scales, it is plausible that the relatively small model spread around the IAV in the Atlantic is related to the fact that most of the simulated IAV is driven by SST-variations (areas with positive correlations in Figure S8b of the Supporting Information S1) and that variations in DIC play a less important role. The strong relationship to SST is also the plausible cause for high correlations between IAV in net sea-air CO_2 fluxes of pCO_2 products and GOBMs in SA STPS and NA STPS. Indeed, when correlating the IAV in net sea-air CO_2 fluxes of pCO_2 products to the IAV in SST (Figure S8a in Supporting Information S1), we find strong correlations in SA STPS and NA STPS biomes. However, in the NA SPSS, the pCO_2 products appear to be more negatively correlated to the IAV in SST (likely driven by DIC variations), in contrast to the GOBMs. This difference in mechanisms over the subpolar gyre is one possible explanation for the disagreement in the IAV in net sea-air CO_2 fluxes between pCO_2 products and GOBMs in the NA SPSS biome.

In the North Atlantic, one of the most prominent climate variability modes at interannual time scales is the NAO. In a study about the influences of NAO on the IAV of North Atlantic CO_2 fluxes, Jing et al. (2019) noted that, in summer, SST is important for the IAV in pCO_2 in the subtropical North Atlantic, while biogeochemical variables probably control the pCO_2 IAV in the subpolar North Atlantic. When relating the IAV of the GOBMs to NAO, we find significant but weak correlations for the NA SPSS and the AEQU biomes ($r = -0.43$, $p = 0.01$ and $r = -0.48$, $p = 0.004$), whereas all other biomes show no significant correlation to the NAO index. However, the pCO_2 products show a similar correlation between NAO and IAV for the AEQU biome ($r = -0.41$, $p = 0.02$), but no significant correlation in the NA SPSS biome (neither for the average nor for single products). The similar correlation in the AEQU is consistent with the fact that in this region, the temperature-driven Atlantic Niño climatic mode plays an important role in modulating the IAV of CO_2 fluxes (Koseki et al., 2023), and that the GOBM - simulated SST variability is well constrained by the observations. The absent correlation in the NA SPSS could be due to the opposing imprints of NAO on pCO_2 in the western and eastern domains of the NA SPSS. In a modeling study, Tjiputra et al. (2012) demonstrated that during positive NAO, SST cooling induces a negative pCO_2 anomaly in the western subpolar gyre, whereas in the eastern part (in the proximity of the Irminger Sea) anomalously deep winter mixing upwells DIC-rich watermasses and induces a positive pCO_2 anomaly (e.g., Fröb et al., 2019). The opposite mechanism is suggested during negative NAO.

We note that despite relatively high correlations between IAV of GOBMs and pCO_2 products in all biomes apart from the NA SPSS (Figure 6c), the amplitude of the IAV of the GOBMs is smaller than that of pCO_2 products in all biomes except the NA STSS (Figure S5 in Supporting Information S1). The amplitude of the IAV of the total sea-air CO_2 fluxes in the Atlantic basin is 0.029 ± 0.01 PgC yr^{-1} (pCO_2 products) and 0.018 ± 0.005 PgC yr^{-1} (GOBMs). These results are significantly different but of similar magnitude to the linear trends of the sea-air CO_2 fluxes of the Atlantic basin (Figure 3). For a better estimate of the sea-air CO_2 fluxes in the Atlantic basin, it is therefore important to have an accurate estimate of both temporal variability and amplitude of the IAV, which is currently not adequately represented. Moreover, the temporal disagreement of IAV of pCO_2 products in the NA SPSS makes it clear that a closer examination of the gap filling methods and their dynamic realism is urgently needed here (Gloege et al., 2021; Hauck, Nissen, et al., 2023).

3.2. Ocean Interior C_{ant} Accumulation From 1994 to 2007

The change in the oceanic storage of anthropogenic carbon (ΔC_{ant}) was evaluated for the period 1994–2007 for comparison between GOBMs, the data-assimilation model OCIMv2021 and two observation-based ΔC_{ant} reconstruction products. All nine considered GOBMs simulated an increase in the basin-wide C_{ant} inventory that is broadly consistent among themselves and with observations (Table S6 in Supporting Information S2). Seven models show high column inventory changes of C_{ant} in the NA SPSS biome and in the NA STSS, consistent with the observation-based ΔC_{ant} reconstructions (Figure S9 in Supporting Information S1), while the other two (PlankTOM12 and CESM-ETHZ) show high ΔC_{ant} column inventories in the vicinity of 35°S, but very weak accumulation in the North Atlantic.

The spatial distribution of the change in column-integrated ΔC_{ant} averaged across the ensemble of nine GOBMs is shown in Figure 7b. Spatial patterns in the ΔC_{ant} column inventory distribution obtained by the OCIMv2021 inverse-model (Figure 7c) are very similar to the GOBM ensemble mean but with higher values throughout the Atlantic, except in the region of the Brazil Current and in the vicinity of the Azores Islands. In addition, OCIMv2021 produces a similar pattern to that obtained from the DIC-based product from Gruber et al. (2019) (Figure 7a), but with stronger (weaker) ΔC_{ant} in the northernmost regions (south of the equator). The GOBM ensemble mean reveals slightly higher ΔC_{ant} column inventories in the subpolar North Atlantic than the observation-based product from Gruber et al. (2019) (Figure 7d). In contrast, over the tropical and South Atlantic, the ΔC_{ant} column inventory of the GOBM ensemble is only about half as high as the reconstruction of Gruber et al. (2019), representing the main discrepancy between both products.

Integrated over the whole Atlantic Ocean, the ΔC_{ant} inventory simulated by the GOBM ensemble (Table 1) is about 28% ± 20% lower than the inventory estimate obtained with the observation-based eMLR(C*) method (Gruber et al., 2019), 17% lower than the age-tracer based method (Khatiwala et al., 2009), and 28% ± 15% lower than the inverse model OCIMv2021. By contrast, the OCIMv2021 ΔC_{ant} inventory is very similar to the estimate from Gruber et al. (2019), while 8% higher compared to that of Khatiwala et al. (2009).

Integrated over the individual biomes of the Atlantic, we found the best agreement between the GOBM ensemble and the estimate from Gruber et al. (2019) in the northern biomes. In the NA SPSS and NA STSS biomes, C_{ant} accumulation rates are very similar between GOBMs, and only two models show extraordinarily low values (50% lower than the GOBMs average; Table S6 in Supporting Information S2). In contrast, OCIMv2021 simulates a ΔC_{ant} inventory that is about 40% higher than the observation-based estimate and the GOBM ensemble mean, and

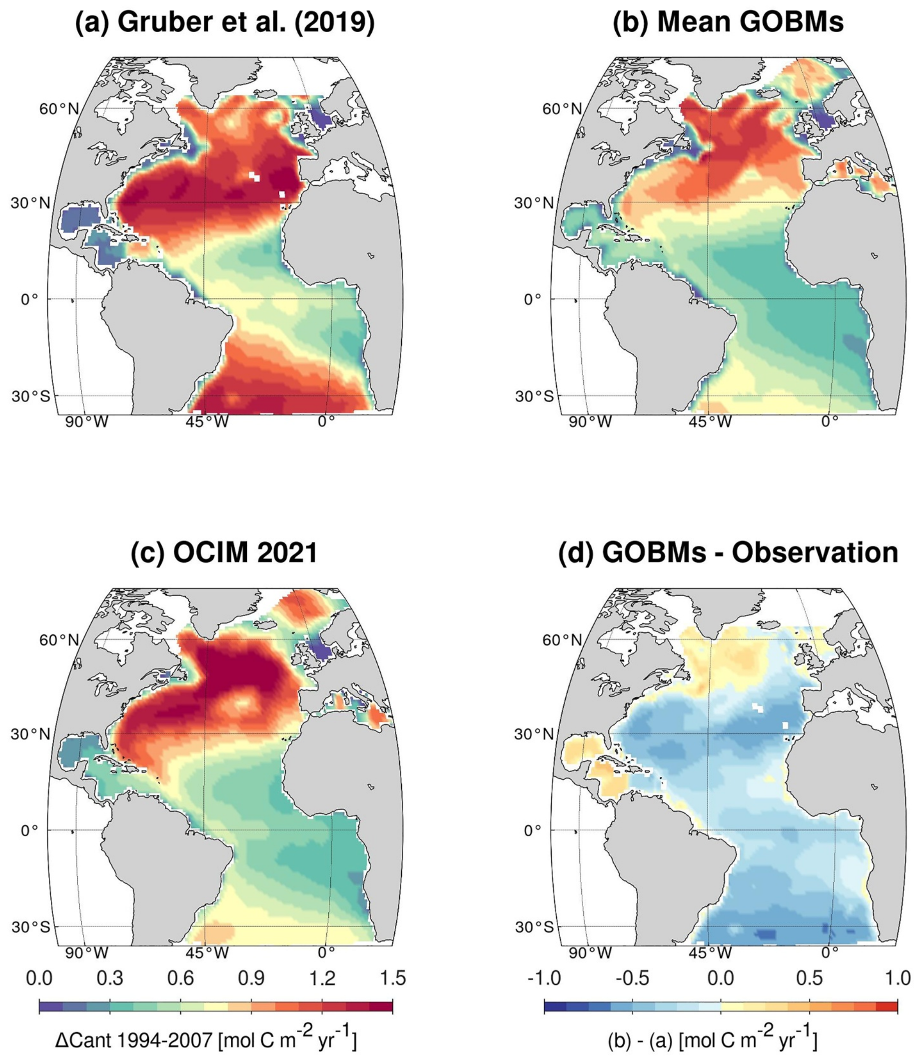

Figure 7. Column inventories of anthropogenic carbon storage changes (ΔC_{ant}), integrated from the surface to 3,000 m from 1994 to 2007. Shown are ΔC_{ant} column inventories for (a) an observation-based reconstruction with the eMLR(C*) method by Gruber et al. (2019); (b) multi-model GOBM ensemble mean; and (c) OCIMv2021. Panel (d) illustrates the difference between the estimates from the GOBM ensemble mean and Gruber et al. (2019).

therefore closer to the values obtained with the Green's Function (Khatiwala et al., 2009). Further south, discrepancies between the GOBM-based and the observation-based ΔC_{ant} inventories increase, bringing the GOBM inventories closer to the age-tracer based product, while OCIMv2021 resembles the eMLR(C*)-based estimates in two of the three remaining biomes. In the NA STPS biome, characterized by the largest inter-GOBM spread, the ΔC_{ant} inventory of the GOBMs is about 25% lower than the observation-based product, while the OCIMv2021 inventory reveals a similar rate of change as the observation-based product. Likewise, in the AEQU biome, the GOBMs' ensemble mean ΔC_{ant} inventory is approximately 30% lower than that from Gruber et al. (2019) and OCIMv2021. The AEQU biome further revealed the lowest ΔC_{ant} inventories with a very narrow inter-GOBM spread. The largest ΔC_{ant} inventory difference between the GOBMs and the observation-based product exists in the SA STPS biome, with a GOBM ΔC_{ant} storage rate nearly 50% lower than that of Gruber et al. (2019). In addition, in the SA STPS biome, the OCIMv2021 ΔC_{ant} inventory is also 30% lower than that of Gruber et al. (2019). No comparison is done for the MED biome because of the lack of data in ΔC_{ant} reconstruction products.

Average ΔC_{ant} vertical profiles of each biome and for the whole Atlantic (Figure S10 in Supporting Information S1) reveal that the maximum ΔC_{ant} occurs near the surface, while the accumulation rates decrease rapidly

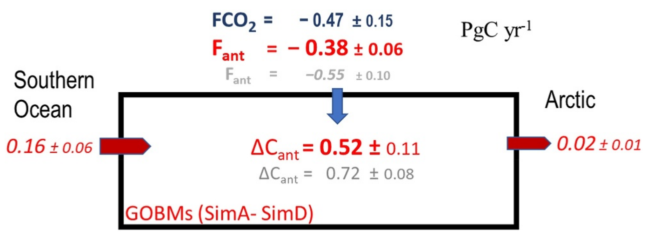

Figure 8. Anthropogenic CO_2 budget in the Atlantic using Simulation A-Simulation D of the GOBMs from 1994 to 2007. The blue arrows indicates sea-air CO_2 fluxes and red arrows indicate lateral transport of C_{ant}. ΔC_{ant} storage changes and sea-air C_{ant} fluxes (Table S7 in Supporting Information S2) are given in red bold numbers. Net sea-air FCO_2 fluxes from GOBMs are given in blue. Red cursive numbers indicate northward C_{ant} transport inferred by the difference between C_{ant} accumulation rate and sea-air uptake. Gray numbers are the ΔC_{ant} estimates from Gruber et al. (2019) and the F_{ant} sea-air flux estimated using the C_{ant} transport of 0.19 ± 0.020 PgC yr^{-1} from Cainzos et al. (2022) at 30°S.

with depth. In general, GOBM simulations and the estimates from Gruber et al. (2019) agree with regard to this vertical distribution, both in the Atlantic and at the biome-level. However, in the NA STPS, AEQU, and SA STPS biomes, the observation-based reconstruction presents a second ΔC_{ant} maximum between 1,400 and 3,000 m depths that is only reproduced by the GOBMs in the NA STPS. Such depth range is associated with waters with moderate values of C_{ant} transported by the DWBC circulating southward below the Antarctic Intermediate Water ΔC_{ant} minimum (Fajar et al., 2015; Rhein et al., 2015; Rios et al., 2003, 2012), mainly North Atlantic Deep Water (NADW). The fact that the GOBMs do not agree with the observations in the southernmost biomes (AEQU and SA STPS) could be indicative of how the GOBMs ventilate the ocean interior below 1,400 m during 1994–2007 period. Updated reconstructions with the eMLR(C*) method by Müller et al. (2023) detect these deep-water accumulations only for the period from 1994 to 2004 but not from 2004 to 2014. These findings could either indicate that (a) ΔC_{ant} in the NADW is subject to larger decadal scale variability than simulated in GOBMs, that (b) the observational data from the 1990s used for the reconstructions from Gruber et al. (2019) as well as the first decade of the reconstruction by Müller et al. (2023) contribute to unidentified biases in the observation-based estimates, or that (c) the statistical gap-filling with the eMLR method approaches its limits in reconstructing the low C_{ant} accumulation rates in these water masses.

3.3. Anthropogenic CO_2 Uptake and Lateral Transport

In terms of recent storage changes in C_{ant}, GOBMs tend to simulate lower accumulation rates than observation-based estimates (Section 3.2), whereas we have previously described that the net CO_2 uptake is larger in GOBMs than pCO_2 products (Section 3.1.1). To assess this apparent inconsistency, the anthropogenic component of the CO_2 fluxes in GOBMs is assessed from the differences of Simulation A minus Simulation D in each GOBM, allowing us to determine the sea-air fluxes caused solely by increased CO_2 in the atmosphere. The anthropogenic FCO_2 averaged across 9 GOBMs (F_{ant}) in the Atlantic as a whole is shown in Figure 8 and for each of the biomes in Figure S11 of the Supporting Information S1. Integrated over the entire Atlantic Ocean, the F_{ant} fluxes are lower in magnitude than the net flux FCO_2 because the natural flux component contributes an additional CO_2 uptake in the NA SPSS and NA STSS biomes. In the other biomes, the natural contributions are lower or even represent positive fluxes (outgassing) (Figure S11 in Supporting Information S1). However, the net result for the Atlantic Ocean is an uptake of natural CO_2 (approx ∼0.1 PgC yr^{-1} obtained from the Simulation B) being transported to the Southern Ocean. In terms of C_{ant}, the biome with the highest uptake is also the NA SPSS, although the latitudinal variability is by far not as marked as in the natural component of FCO_2.

Knowing the C_{ant} accumulation rate in the ocean interior and the flux entering from the atmosphere, we can infer horizontal transport rates (Figure 8; Figure S11 in Supporting Information S1). Given the enclosed bathymetry of the Mediterranean Sea, the GOBM ensemble simulates a mean net export of C_{ant} from the Atlantic to the Mediterranean of 0.0055 ± 0.0050 PgC yr^{-1}, inferred as the residual between an accumulation rate of 0.018 PgC yr^{-1} and C_{ant} uptake from the atmosphere at a rate of −0.012 PgC yr^{-1} (Figure S11 in Supporting Information S1). This inferred C_{ant} import to the Mediterranean Sea is consistent with the observation-based transport estimates in the Strait of Gibraltar of 0.0042 ± 0.0010 PgC yr^{-1} (Huertas et al., 2009).

From estimates of the exchange between the Nordic Seas and the Arctic (Jeansson et al., 2011) and the exchange from the Nares Strait, a net flux to the Arctic of 0.02 ± 0.01 PgC yr^{-1} was estimated. Thus, the remaining lateral transport rates between the different biomes were estimated for each GOBM as the difference between surface flux, interior accumulation and the boundary fluxes. From the average of the GOBM results (lateral C_{ant} transport and F_{ant}, Figure S11 in Supporting Information S1), the average transport from the Southern Ocean is obtained (Figure 8).

For the Atlantic, the northward transport of C_{ant} from the Southern Ocean decreases northward to almost zero (Figure S11 in Supporting Information S1) or reverses sign at the boundary between the NA STSS and NA SPSS biomes. These C_{ant} transports are fully compatible with the AMOC, in which the upper branch transports more

C_{ant} northward than the southward lower branch, and also with the decrease of the vertical gradient of C_{ant} northward such that in the NA SPSS biome the vertical gradient of C_{ant} is small (Figure S10 in Supporting Information S1). With these results, the net transports of 0.163 ± 0.057 PgC yr^{-1} at the South Atlantic boundary obtained from the GOBM results are consistent with recent transports estimated from ocean sections at 30°S of 0.186 ± 0.019 PgC yr^{-1} (Cainzos et al., 2022). This suggests that the weak anthropogenic sea-air CO_2 fluxes are the primary cause of low ΔC_{ant} in the South Atlantic. The lower ΔC_{ant} in the interior ocean and in particular in the NA STPS and SA STPS biomes suggest that the anthropogenic contribution to the total FCO_2 in GOBMs is 30% weaker than expected from C_{ant} observations in the interior ocean. Although the total FCO_2 obtained from GOBMs is stronger in the Atlantic than those derived from pCO_2 products, we note that the total FCO_2 from the GOBMs contains no RCO correction here. While our estimate of the anthropogenic contribution is unaffected by RCO, this is not true for the FCO_2 estimates of the GOBMs. If we were to apply the RCO-values based on Regnier et al. (2022) and Lacroix et al. (2020) to the FCO_2 estimates of the GOBMs, then their total FCO_2 estimate would be weaker than that derived by the pCO_2 products.

The inferred northward C_{ant} transport at the southern boundary between Atlantic and Southern Oceans obtained for each of the nine GOBMs with Simulations A and D shows a high correlation ($r^2 = 0.61$; p-level < 0.01) with the maximum AMOC values at 26°N of each of these GOBMs (Figure S12 in Supporting Information S1), indicating that the northward physical transport is the main driver of the northward C_{ant} transport. We note additionally that, in comparison with observations, the GOBMs tend to underestimate the maximum AMOC values at 26°N (Figure S12 in Supporting Information S1) and hence the inferred northward C_{ant} transport (Terhaar et al., 2024).

4. Discussion

4.1. Progress Since RECCAP1

Over the last decade, the nature of the pCO_2 products has changed significantly, not only because of a significant growth in the number of observations (Bakker et al., 2016) but also because of the implementation of new data interpolation methodologies (e.g., Denvil-Sommer et al., 2019; Gregor et al., 2019; Rödenbeck et al., 2015), and improvements in the fidelity of predictor variables. This led to RECCAP2 being able to use nine different pCO_2 products with time-varying FCO_2 estimates. RECCAP1 only had 2 products available for time-varying Atlantic Ocean FCO_2 estimates: a multi-parameter regression based on the gridded product of SOCATv1.5 (Pfeil et al., 2013) as well as regional scale FCO_2 estimates based on the pCO_2 database analysis of McKinley et al. (2011). Additionally, the climatology of Takahashi et al. (2009) formed a cornerstone of the RECCAP1 studies and has proven to be a very robust product, with estimates close to the climatology obtained from the new pCO_2 products. On the modeling side, there have also been many relevant advances between RECCAP1 and RECCAP2. In RECCAP1, only six models were used, while RECCAP2 employs almost twice the number of models. A subset of the available GOBMs in RECCAP2 also participated in RECCAP1 and have been improved in both physical and biological processes (e.g., Aumont et al., 2015; Schwinger et al., 2016; Wright et al., 2021), with an enhanced spatial resolution (e.g., from ∼2° to ∼1°), though they remain too coarse to resolve mesoscale processes.

A direct comparison between RECCAP1 and RECCAP2 estimates of the Atlantic cannot be performed due to the appreciable improvements in methods and data coverage. Moreover, the estimates made in RECCAP1 have a different regional domain (spanning from 44°S to 79°N). The zonal region from 35°S to 44°S is no longer part of the Atlantic Ocean mask in RECCAP2, but instead considered to be part of the Southern Ocean (Hauck, Gregor, et al., 2023). In addition, the time period covered in RECCAP1 spans the years 1990–2009, while RECCAP2 covers the years from 1985 to 2018 and considers not only the whole time-period but also two sub-periods (before and after 2000). In RECCAP1, an estimate of RCO flux component (0.17 ± 0.04 PgC yr^{-1}) was subtracted from the FCO_2 values obtained for GOBMs (see Table S8 in Supporting Information S2 for details), which was not performed here. However, to allow a direct comparison with RECCAP1 (Table S8 in Supporting Information S2), we additionally calculated FCO_2 averages for the region from 44°S to 79°N for the RECCAP1 time period. To compare the GOBM estimates, we additionally re-added the RCO-flux to the RECCAP1 estimate. Our inferred RECCAP2-results for the FCO_2 averages are similar to those published in RECCAP1 (Schuster et al., 2013) as the FCO_2 estimates are within the uncertainty of each other (Table S8 in Supporting Information S2). Yet, the mean FCO_2-values increased in both the GOBM ensemble mean (21% increase) and pCO_2 product ensemble average (9% increase). Both the RECCAP1 as well as the RECCAP2 estimate show a higher average FCO_2-value for the GOBMs, yet the mean difference between GOBMs and pCO_2 products is larger in RECCAP2.

It is difficult to compare estimates of decadal trends between RECCAP1 and RECCAP2, as RECCAP1 only provided upper-bound estimates for the trends based on the pCO_2-database. The GOBMs of RECCAP1 estimated the largest trends in FCO_2 for the North Subtropics and estimated the trends for the other Atlantic regions to be negligible or very small (Schuster et al., 2013). We cannot confirm this in RECCAP2 (Figure 4) because our trend estimates consider different time-periods and that the IAV could additionally influence the trend-estimates substantially (e.g., Figure 4).

For the IAV in FCO_2, Schuster et al. (2013) found in RECCAP1 significant but weak correlations to the NAO for the Equatorial biome with opposing signs between GOBMs ($r = -0.43$) and pCO_2 products ($r = 0.35$), potentially relating to their IAV being driven by SST-variations and DIC-variations, respectively. Here, the new definition of the Equatorial biome in RECCAP2 helps to confine the upwelling region such that the IAV in this region is DIC driven in both GOBMs and pCO_2 products, with correlations of $r = -0.40$ and $r = -0.47$ with the NAO, respectively. In our case, negative correlations indicate DIC-driven variations as we correlate the NAO with the sea-to-air flux, while Schuster et al. (2013) correlated it with the air-to-sea flux (i.e., flux of opposite sign). However, the issue of the GOBMs being more SST-driven remains also within the IAV of RECCAP2, most notably in the North Atlantic subpolar gyre.

In terms of FCO_2 seasonality, the southern subtropical regions, the equatorial region and the northern subtropics studied in RECCAP1 followed the seasonal increase and decrease of pCO_2 driven mainly by warming and cooling in both GOBMs and observation-based estimates. These general results remain consistent in our analysis. In the NA SPSS, the RECCAP1 pCO_2 products showed that the seasonal cycle is reversed with a minimum during summer and outgassing in winter (Schuster et al., 2013), conforming to direct observations (Olsen et al., 2008), whereas the seasonal cycle of GOBMs was dominated by the temperature component. As the Atlantic regions in RECCAP1 were defined simply via latitudinal boundaries, Schuster et al. (2013) denoted that the temperature controlled seasonal cycle of the GOBMs is likely due to the inclusion of the northern reaches of the subtropical gyre. The refinement of the Atlantic regions in RECCAP2, however, shows that biogeochemical boundaries with a clearer exclusion of the subtropical gyre do not change the temperature control of the seasonal cycle of the GOBMs in the NA SPSS.

Even though RECCAP2 benefits from a substantial increase in observations and improvements in modeling (complexity and resolution), the mean difference between GOBMs and pCO_2 products is larger in RECCAP2 and the disagreements between pCO_2 products and GOBMs in the NA SPSS remain in terms of IAV and seasonal cycle. Potential mechanisms for this are further discussed in Section 4.3.

4.2. The Influence of the Riverine CO_2 Outgassing on Comparisons of the CO_2 Sink in RECCAP2 Models and Observation-Based Products

When averaged over the 1985 to 2018 period, the mean FCO_2 of pCO_2 products and GOBM ensemble agree within the ranges of their ensemble spread for most of the biomes and the Atlantic basin (Table 1). The related spatial distribution of FCO_2 also agrees with respect to the large-scale, basin-wide patterns (Figure 1), although some discrepancies are detected in the NA SPSS biome. The average Atlantic FCO_2 estimated by the GOBM ensemble is 30% lower than the estimate from pCO_2 products.

The riverine carbon outgassing (RCO, see Section 2.4) hampers the comparison of the FCO_2 estimates from the GOBMs with those of pCO_2 products, since the input of riverine carbon and the burial of carbon is treated in various ways across the ensemble of GOBMs. Furthermore, relevant output from the GOBMs is missing to properly assess the contribution of carbon, alkalinity and nutrient input from land and their burial in sediments, resulting in a situation where only a rough approximation of the RCO in the GOBMs is possible (Terhaar et al., 2024). In the RECCAP2 protocol, it was recommended to apply the spatial distribution of the RCO of Lacroix et al. (2020), scaled to a globally integrated RCO value of 0.65 ± 0.3 PgC yr^{-1} (Regnier et al., 2022). This procedure results in a large adjustment of 0.27 ± 0.06 PgC yr^{-1} (3.9 ± 1.0 mol C m^{-2} yr^{-1}) for the Atlantic sea-air CO_2 flux, which is more than half of the FCO_2 derived from the set of GOBMs and 70% of that estimated from pCO_2 products (in absolute numbers). Although other estimates of the RCO reported by Aumont et al. (2001) and Jacobson et al. (2007) reduce the RCO in the Atlantic by 1/3, the relative magnitude of the RCO compared to the FCO_2 from GOBMs and pCO_2 products remains substantial.

In the Atlantic Ocean, the difference between the FCO_2 obtained from the ensemble pCO_2 products and the ensemble of GOBMs is 0.10 ± 0.11 PgC yr^{-1}. The RCO derived from Aumont et al. (2001), Jacobson et al. (2007), and Lacroix et al. (2020) scaled up to Regnier et al. (2022) are 0.16 ± 0.05, 0.16 ± 0.04, and 0.27 ± 0.06 PgC yr^{-1}, respectively (Table S3 in Supporting Information S2), yielding an ensemble average of 0.20 ± 0.05 PgC yr^{-1}. All four of these values are higher than the average difference between the pCO_2 products and GOBMs, although within the combined uncertainty of all estimates. Importantly, for four of the five biomes (NA SPSS, NA STSS, AEQU, and SA STPS), the ensemble RCO-estimates agree well with the FCO_2 differences (pCO_2 products minus GOBMs) with a mean difference of only −0.001 ± 0.019 PgC yr^{-1} when the ensemble of RCO is added to the GOBMs estimate (last column in Table S3 of the Supporting Information S2).

The biome with the largest discrepancy between FCO_2 in the GOBMs and in the pCO_2 products is the NA STPS. Likewise, the three estimates of the RCO diverge most in this biome, indicating a high RCO-uncertainty. The FCO_2 difference between pCO_2 products and GOBMs would require an RCO of −0.024 ± 0.013 PgC yr^{-1} to be balanced, that is, an additional CO_2 uptake rather than outgassing due to riverine input of carbon. However, this difference is of reversed sign and much lower than the ensemble mean of the direct RCO estimates (+0.073 ± 0.048 PgC yr^{-1}, Table S3 in Supporting Information S2). This discrepancy would be even larger when the RCO estimate recommended in RECCAP2 (+0.126 ± 0.010 PgC yr^{-1}) was used. At the same time, the ΔC_{ant} (Table 1) and F_{ant} rates of the GOBMs in the NA STPS biome are lower than an observation-based estimate from Zunino et al. (2015), who used DIC measurements along the 26.5°N and 7.5°N sections from 1992/93 and 2010/11, and inferred a F_{ant} of −0.23 ± 0.02 PgC yr^{-1} over an area of 15.3 × 10^{12} m^2 (70% of NA STPS), which is more than twice the estimated F_{ant} in the GOBMs (−0.084 ± 0.010 PgC yr^{-1}, Figure S11 in Supporting Information S1). The F_{ant} difference between the GOBMs and the observation-based estimate from Zunino et al. (2015) is very similar to the difference between the direct RCO estimate (+0.126 ± 0.040 PgC yr^{-1}) and the residual between the FCO_2 from pCO_2 products and GOBMs (−0.024 ± 0.013 PgC yr^{-1}). This agreement in the differences suggests that the GOBMs indeed underestimate the C_{ant} uptake in the NA STPS biome. If the GOBMs simulated a substantially stronger C_{ant} uptake (by about −0.1 PgC yr^{-1}), then the direct RCO estimate would plausibly explain the FCO_2 difference between the GOBMs and pCO_2 products, albeit with large uncertainty. The likely underestimation of F_{ant} by the GOBMs in the NA STPS biome is further supported by their ΔC_{ant} that is only about half as large as the observation-based estimate from Gruber et al. (2019) (Table 1), as well as the lower northward C_{ant} transport compared to two observation-based estimates (Brown et al., 2021; Cainzos et al., 2022).

4.3. Temporal Variability in Sea-Air CO_2 Fluxes in Models and pCO_2 Products

In the results section, differences between models and pCO_2 products in sea-air CO_2-flux dynamics are described in terms of trends, seasonality and interannual variability. The region where the GOBMs and pCO_2 products show the largest discrepancies is the NA SPSS: the biome with the highest CO_2 uptake rates. When looking at the seasonal decomposition of surface pCO_2, it becomes clear that the seasonality is primarily temperature-driven in the GOBMs so that their CO_2 uptake is larger in winter than in summer because of the seasonal SST changes. The seasonal cycle of the pCO_2 products is driven by DIC variations (for more information see Figure S4 in Supporting Information S1; Rodgers et al., 2023). In the North Atlantic subpolar gyre, direct observations of interannual variability in winter pCO_2 have shown that this is associated with variations in mixed layer depths in this season (Fröb et al., 2019). That means that more intense mixing during colder winters leads to higher surface DIC and consequently higher pCO_2, and thus a reduced flux of CO_2 into the ocean. A DIC-driven dynamic is supported by the seasonal cycle of the pCO_2 products and the strong, negative correlation of the pCO_2 product between the IAV of CO_2 flux and SST in this region (Figure S8a in Supporting Information S1). On the other hand, the GOBMs simulate positive correlations between the IAV of CO_2 flux and SST. Hence the disagreement between pCO_2 products and GOBMs in IAV and seasonal cycle is interconnected and driven by the same cause: SST-driven temporal variations in the GOBMs versus DIC-driven temporal variations in the pCO_2 products. We note that the NA SPSS is also the region in which pCO_2 products and GOBMs have the largest disagreement in their mean CO_2-fluxes and the largest uncertainty in their CO_2-trends (see Figures 1 and 4).

When looking for the underlying causes for the disagreement in seasonal driving forces and IAV between pCO_2 products and GOBMs in the NA SPSS, we find that most of the GOBMs for which the simulated AMOC is available show significant correlations between their IAV of CO_2 fluxes in the NA SPSS and AMOC-variations with correlation between −0.38 and −0.53. Further, using Earth System Models, Goris et al. (2023) showed that the AMOC-strength drives the simulated seasonal variability in the North Atlantic. Altogether, this suggests that the underestimation of the AMOC in the GOBMs (Terhaar et al., 2024) could be an underlying cause for the underestimation of the role of biogeochemical variability for both IAV and seasonality by the GOBMs in the NA SPSS.

Furthermore, we identify that the comparatively small DIC variations (as seen in both seasonal cycle and IAV) in the GOBMs might also be a consequence of their current simplified set-up, or the total lack, of riverine carbon fluxes (Terhaar et al., 2024). According to Aumont et al. (2001) and Gao et al. (2023), the contribution of RCO weakens the CO_2 uptake in the NA subpolar gyre and in the Southern Ocean. In fact, applying the predicted riverine carbon outgassing of Aumont et al. (2001) to the NA SPSS biome removes the difference in FCO_2 mean fluxes (1985–2018) between pCO_2 products and GOBMs (Table S3 in Supporting Information S2). The RCO modeled by Aumont et al. (2001) also shows a similarity (in numbers) to the mean FCO_2 differences (1985–2018) between GOBMs and pCO_2 products in the NA STSS, AEQU, and SA STPS biomes (Table S3 in Supporting Information S2). The study of Aumont et al. (2001) highlights the importance of the slow reactivity of dissolved organic carbon (DOC) supplied by rivers to the regional distribution of RCO, which hence might also contribute significantly to seasonal and interannual variability.

Finally, the different strengths of drivers and the resulting large disagreements in IAV between GOBMs and pCO_2 products may leave an imprint on the calculated trends of the sea-air CO_2-fluxes of the NA SPSS biome for the period 2001–2018 (Figure 4). Here, the pCO_2 products show an accelerated trend for the period 2001–2018 which is not simulated by the GOBMs. Similarly, the IAV of the pCO_2 products is in a positive phase in the year 2000 and in a negative phase in the year 2018 in the NA SPSS (Figure 6), which is not the case for the GOBMs. While this behavior is especially pronounced in the NA SPSS, the NA STPS biome shows a similar phasing in its IAV when comparing GOBMS and pCO_2 products. In a previous study (McKinley et al., 2020), it was found that the IAV is a potential driver of differences in trends between observational products and GOBMs.

While the IAV has an influence on the decadal trends, it cannot solely explain that the calculated trends of sea-air CO_2 fluxes before and after the year 2000 are similar across our ensemble of GOBMs, while the trends obtained from surface CO_2 observations show a sharp increase between the trends of the pre- and post-2000. We advise caution when comparing the CO_2 trends before the year 2000 between GOBMs and pCO_2 products, as the trends of the pCO_2 products are strongly conditioned by the FCO_2 estimates in the early years (Figure S2 in Supporting Information S1), where the available observations (pCO_2 data and predictors) to generate the pCO_2 products are far less, such that the estimates of the pCO_2 products agree less than in later years (Figure 3; Figure S2 in Supporting Information S1). In fact, the pCO_2 products do not agree on the CO_2 trends before the year 2000 (-0.024 ± 0.075 PgC-yr^{-1} dec^{-1}) with three pCO_2 products suggesting a weakening of the CO_2 uptake in the Atlantic before 2000 and four pCO_2 products a strengthening (Table S5 in Supporting Information S2). For the trends after the year 2000, the agreement of the pCO_2 products allows for a more confident estimate of a strengthening CO_2 sink in the Atlantic with a trend of -0.126 ± 0.031 PgC-yr^{-1} dec^{-1}, which is twice the trend estimated by the GOBMs, of -0.060 ± 0.017 PgC-yr^{-1} dec^{-1}. Nevertheless, by using one of the pCO_2 products (MPI-SOM-FFN) in a model, it has been shown that a bias in sampling locations influences the trends and an optimal sampling strategy reduces the negative trend estimate in the northern hemisphere for the years 2000–2018 (Hauck, Nissen, et al., 2023). Hence, a skewed sampling strategy could potentially influence the 2000–2018 trend estimate of the pCO_2 products. For the GOBMs, we want to note that their simulated seasonal cycle might lead to a trend estimate that is too low, as it has been shown for an ensemble of Earth System Models that a more SST-driven seasonal cycle is related to a shallower MLD and a less vivid AMOC (Goris et al., 2018, 2023). Earth System Models with a weaker AMOC simulate more warming and less future carbon uptake in the North Atlantic. Contrarily, a biology-driven seasonal cycle will lead to enhanced carbon uptake due to the increasing sensitivity of pCO_2 to DIC variations with declining buffer capacity of the ocean (Hauck & Völker, 2015).

4.4. C_{ant} Storage and Transport

In the Atlantic, the GOBM ensemble C_{ant} accumulation rate (1994–2007) is 28% ± 20% lower than the observation-based estimate of Gruber et al. (2019). In general, both GOBMs and the Gruber et al. (2019) product show maximum C_{ant} concentrations near the surface with a rapid decrease toward depth. Nevertheless, surface GOBM estimates are in general slightly lower than the observation-based product, which might be related to biases in the Revelle factor caused by too high pre-industrial CO_2 values in a couple of GOBMs with a late starting date past 1765 (Terhaar et al., 2024). The highest agreement between GOBMs and the observation-based product in ΔC_{ant} is found north of 30°N, while the GOBMs simulate systematically lower accumulation rates in the South

10.1029/2023GB007862

Atlantic (Figure 7, Table 1). In the upper ocean layer, where the upper limb of the AMOC is located, the differences in ΔC_{ant} are not particularly evident (Figure S10 in Supporting Information S1). However, between 1,400 and 3,000 m depths, GOBMs do not reproduce the C_{ant} peak estimated by the observation-based product (Fajar et al., 2015; Gruber et al., 2019; Rhein et al., 2015; Rios et al., 2012) for the Atlantic (Figure S10 in Supporting Information S1) and, more specifically, for the AEQU and SA STPS biomes. This depth interval, with lower ΔC_{ant} in GOBMs compared to the observation-based estimate, coincides with the depth at which the NADW is located. This result suggests that over the 1994–2007 period, the GOBMs simulated too little C_{ant} advection into the South Atlantic within the Deep Western Boundary Current that carries the C_{ant}-rich NADW toward the Southern Hemisphere (Goris et al., 2023). This interpretation would be consistent with the fact that most of the RECCAP2 GOBMs simulate too weak AMOC strengths (Terhaar et al., 2024). In addition, we note that biased low C_{ant} uptake in the Southern Ocean (Hauck, Gregor, et al., 2023), and the subsequent northward transport to the Atlantic, could also contribute to the too-low ΔC_{ant} in the South Atlantic by GOBMs. However, the transport of C_{ant} from the Southern Ocean to the Atlantic is in accordance with the observations (Cainzos et al., 2022). We also note that the GOBMs may underestimate the temporal variability of the ocean interior transport, since the ΔC_{ant} of the GOBMs in the South Atlantic are more similar to the estimates by Khatiwala et al. (2009), which assumes a quasi-stationary ocean circulation (see Table 1 for SA STPS biome). In contrast, the GOBMs show a lower decadal variability of the ΔC_{ant} than observation-based products (Gruber et al., 2019; Müller et al., 2023). The interannual variability of the ΔC_{ant}, derived from the linear regressions, is typically 1.5% ± 1.0% of the absolute increase rates across all biomes and the whole Atlantic Ocean, indicating that the ΔC_{ant} in the GOBMs occurs as a rather steady process.

The assessment of C_{ant} accumulation and transport in the Atlantic conducted in RECCAP1 (Khatiwala et al., 2013) revealed that the largest anthropogenic CO_2 uptake occurs in the Southern Ocean, with much of this uptake being transported equatorward through the Antarctic Intermediate Water and Subantarctic Mode Water. Most of this C_{ant} is stored in the SA STPS (Mikaloff Fletcher et al., 2006). There is also a significant C_{ant} uptake in the tropical Atlantic that is partially transported southward, but most of it is stored in the tropics or transported northward. The C_{ant} taken up in the North Atlantic is transported northward in the upper limb of the AMOC and subsequently entrained to the NADW and transported southward in the lower limb of the AMOC. The GOBMs analyzed here confirm these spatial patterns of ΔC_{ant} (though accumulation is low in the South Atlantic below 1,500 m, Figure 7; Figures S9 and S10 in Supporting Information S1) and of meridional transport (dominated by inflow from the Southern Ocean, Figure 8; Figure S11 in Supporting Information S1).

Khatiwala et al. (2013) stated that the C_{ant} transports estimated from GO-SHIP sections using hydrographic data and observation-based C_{ant} estimates (Álvarez et al., 2003; Holfort et al., 1998; Macdonald et al., 2003; Pérez et al., 2013; Rosón et al., 2003) represent C_{ant} transport at a single time point. Such C_{ant} transport estimates may be biased because seasonal variability is not resolved (Wilkin et al., 1995). However, recent estimates cover long time series (Brown et al., 2021), or aim to provide decadal climatological estimates (Cainzos et al., 2022). In RECCAP1, Khatiwala et al. (2013) showed that C_{ant} transports, obtained based on GOBMs and from hydrographic sections, exhibit similar C_{ant} transports between 44°S and the Equator with a northward transport of 0.15–0.20 PgC yr^{-1}, but, in contrast, in the North Atlantic, the GOBMs simulated a gradual northward decrease of the C_{ant} transport, reaching zero horizontal net transport between 35° and 60°N. This pattern is confirmed in RECCAP2 (Figure S11 in Supporting Information S1) with a larger number of GOBMs involved. Estimates of C_{ant} transport at 26°N along transoceanic sections (Brown et al., 2021; Cainzos et al., 2022; Macdonald et al., 2003; Pérez et al., 2013; Rosón et al., 2003; Zunino et al., 2015) showed larger values than those of the oceanic inversion or GOBMs. These discrepancies remained uncertain in RECCAP1 due to the uncertainties in the hydrographic estimates and the difficulties in directly comparing the two techniques. However, one must also consider the difficulties that inverse models and GOBMs have in representing mesoscale processes, mainly in regions of very intense currents such as the Florida Current, Gulf Stream, and DWBC (Bower et al., 2019; Hirschi et al., 2020; Khatiwala et al., 2013; Ma et al., 2016).

Recent estimates by Brown et al. (2021) using the RAPID long time series (2004–2012), with an assessment of C_{ant} transports at 10-day timescale, confirm a strong C_{ant} transport at 26.5°N of 0.191 ± 0.013 PgC yr^{-1}, which is in the middle of the range (0.128 ± 0.032 to 0.25 ± 0.05 PgC yr^{-1}) of the eight estimates obtained from five sections between 1992 and 2011 (collected in Cainzos et al. (2022)). The ensemble average C_{ant} transport over 26°N obtained for the nine GOBMs used here is 0.053 ± 0.037 PgC yr^{-1}, which is almost four times lower than the C_{ant} transport of Brown et al. (2021). Racapé et al. (2018), using a global NEMO-PISCES model with a finer spatial resolution (0.5° × 0.5°), obtained a northward transport of 0.092 ± 0.04 PgC yr^{-1} somewhat closer to observation-based estimates, suggesting that the spatial resolution of the GOBMs is relevant for the simulation of ocean interior transport. Observational-based evaluations of C_{ant} transport indicate the dynamical difficulties that CMIP5/6 climate models in certain regions have in achieving realistic simulations of the AMOC and DWBC, when run at relatively coarse resolutions on the order of 1° (Hirschi et al., 2020; Ma et al., 2016), which does not allow to correctly simulate vertical structures nor to resolve mesoscale ocean eddies (Bower et al., 2019). For the RECCAP2 GOBMs, it was shown that the AMOC is, on average, underestimated by 3.1 ± 5.2 Sv at 26.5°N, which can partly explain this discrepancy between GOBMs and observation-based estimates (Terhaar et al., 2024).

The weak C_{ant} northward transport in the subtropical region as shown by GOBMs might also be connected to a possible mismatch in C_{ant} uptake in the NA STPS biomes (Zunino et al., 2015) described above. Despite the agreement in mean FCO_2 between pCO_2 products and GOBMs in the NA STPS, the mismatch between the potentially strong RCO (Table S3 in Supporting Information S2) and the "residual RCO" (difference between GOBMs and pCO_2 products) further supports that the GOBMs simulate a too low C_{ant} uptake (Table S3 in Supporting Information S2) despite the apparent agreement in the net flux. The reduced C_{ant} uptake would be conveyed both northward and downward to the ocean interior. In fact, Cainzos et al. (2022) show that the contribution of vertical mixing is somewhat larger than the southward horizontal advection of ΔC_{ant} in the lower limb of AMOC. Therefore, the insufficient incorporation of the RCO in the GOBMs may also result in a lower CO_2 uptake, and at the same time also generates an excess CO_2 uptake in the NA SPSS (Aumont et al., 2001; Gao et al., 2023).

4.5. Future Recommendations

Observations of pCO_2 in the Atlantic Ocean have greatly improved over the past two decades, making it one of the most densely sampled oceans temporally and spatially. However, the surface pCO_2 observations are highly skewed in space and time, potentially inducing spurious results in the gap-filling algorithms used for estimating CO_2 fluxes. In fact, even in the well sampled Atlantic, the observations cover less than 10% of all 1° × 1° by 1-month grid points, requiring the gap filling methods to fill more than 90% of the grid cells. Recent studies with synthetic model data using similar resolution and parameterizations to observations (Gloege et al., 2021; Hauck, Nissen, et al., 2023) indicate that gap-filling methods may be prone to a possible overestimation of the decadal rates of increase in CO_2 uptake when data are sparse, partially explaining the discrepancy between these products and GOBMs. We also note that in the data-sparse period 1985–2000, the trends generated by the various observation-based products were highly correlated with their flux estimate in 1985. This shows that with reduced observational coverage, the trend in the products tends to drift apart. Therefore, data-coverage as well as gap-filling methods need to be improved to reduce uncertainties in the trends. It is now quite worrisome that key Atlantic ship of opportunity lines for surface ocean pCO_2 observations have been lost or operated with reduced capacity in the past years—this tendency must be reversed if we want to retain our ability to accurately constrain the Atlantic Ocean CO_2 sink and its variability. Another aspect is the lack of funding in SOCAT itself, resulting in a longer time lag before collected data gets included in the database (https://www.ioccp.org/images/Gnews/2023_A_Case_for_SOCAT.pdf).

This assessment relies on simple bulk flux formulations used in pCO_2-based products and GOBMs to determine FCO_2 from ΔfCO_2 fields with little regard to interfacial processes controlling gas fluxes. Gas transfer is based on a global parameterization with wind speed. Recent advances in direct flux estimates provide the opportunity to use regionally resolved gas transfer estimates (Blomquist et al., 2017; Butterworth & Miller, 2016). Yang et al. (2022) show clear regional variation in the K660-wind speed relationship, which can explain some of the regional differences observed between GOBMs and pCO_2 products. Near-surface CO_2 concentration gradient impact fluxes as well as shown herein by applying a cool skin effect. Further improvements in characterization of these gradients will improve the quantification of CO_2 fluxes (Dong et al., 2022). Of note is that the effect of gas transfer and near-surface gradients will be less in GOBMs than pCO_2 products because of the inherent feedback between fluxes and concentration gradients in GOBMs (Bellenger et al., 2023).

The Atlantic Ocean is characterized by high temporal dynamics not only in the surface layer but also in the deep layers connecting the North Atlantic to the Southern Ocean through the deep western boundary current. This involves strong mesoscale and sub-mesoscale dynamic currents and structures. The effectiveness of GOBMs in representing dynamic climate change processes is highly dependent on their spatial and temporal resolutions.

10.1029/2023GB007862

Current spatial resolution can barely reproduce the dynamics of strong CO_2 transport in the Atlantic, as well as ocean-coastal interactions.

A number of future model improvements could further address or minimize the discrepancies in the interior C_{ant} inventory estimates. As simulations of the ocean biogeochemistry are strongly constrained by the performance of the physical model (Doney et al., 2004), more detailed assessments should be carried out of key physical dynamics that govern the surface to deep carbon transport, such as the representation of mode water and intermediate and deep waters in the North Atlantic (Racape et al., 2018). Assessment of GOBMs' ability to simulate observed episodic ventilation events and their impact on interior C_{ant}, for example, as documented in Rhein et al. (2017) and Fröb et al. (2016), could shed additional light on their validity. Through winter convective mixing, biases in the interior carbon chemistry can influence the upper ocean carbon uptake capacity in models due to biases in the buffering capacity of the ocean (Terhaar et al., 2022; Vaittinada Ayar et al., 2022). Improvements in the representation of mixing by the models would likely also alleviate the issues with the simulated amplitude and timing of spring bloom and winter remineralization in the subpolar region (that we identified as key deficiencies in GOBMs) and further improve their FCO_2 seasonal cycle. Better observational constraints and improvement in mixing parameterizations are needed to alleviate this issue. Higher spatial resolution is likely necessary to improve key upper ocean physical features in the Atlantic Ocean, such as the Gulf Stream (Chassignet et al., 2020), which has been shown to play a significant role in constraining the seasonality and trends of North Atlantic carbon fluxes and interior sequestration (Goris et al., 2023). Results from the high-resolution regional model (ROMS-ETHZ) indicate a better representation of the FCO_2 seasonal cycle in the NA SPSS and a better representation of the trends for 2001–2018 in NA SPSS, NA STSS and SA STPS, while we see no improvement or even a worse representation in other regions. A detailed and overarching investigation of the benefits of higher resolution for the carbon cycle would be desirable. Further, as the number of observations continues to increase, improvements in biogeochemical parameterizations can be achieved through data assimilation, for example, to address the regionally heterogeneous biological processes (Gharamti et al., 2017; Tjiputra et al., 2007). In addition, improvement in biological model complexity may be needed to optimally reproduce the observed biogeochemical dynamics across spatially varying regimes such as the Atlantic basin (Gehlen et al., 2015). The interior lateral transport of C_{ant} is projected to play an increasing role in the future (Tjiputra et al., 2010). Better constraints of the northward (and southward) transport of anthropogenic CO_2 in the ocean, through the upper (and lower) limb of the AMOC should be considered to improve estimates of fluxes further north (Cainzos et al., 2022). Finally, an improved model experiment protocol that includes a multi-centennial preindustrial spin up (Séférian et al., 2020), common initialization procedure, and implementation of the river carbon loop should be considered (see also Terhaar et al., 2024).

In the North Atlantic, Fontela et al. (2020) showed that semi-refractory DOC mineralization in the lower limb of AMOC represents a significant contribution to DIC of the same order of magnitude as CO_2 exchange with the atmosphere, resulting in a possible CO_2 source that could explain the differences observed between the observed FCO_2 (Takahashi et al., 2009) and those estimated by inverse methods (Gerber et al., 2009; Gruber et al., 2009; Mikaloff Fletcher et al., 2007). In RECCAP, the role of DOC has not been evaluated, nor the double impact of its seasonal cycle, that is, diverting DIC which reduces pCO_2 in summer or by DOC deep mineralization, increasing DIC transport. Semi-refractory DOC is exported to the mesopelagic zone and even deeper depths in the North Atlantic, as documented by Hansell (2013), who estimated ~0.34 PgC yr^{-1} DOC export, with a mineralization time scale to CO_2 of decades. In the North Atlantic, the coupling between DOC production and export is revealed in the export of locally produced DOC (Fernandez-Castro et al., 2019; Roshan & DeVries, 2017). In fact, the carbon sequestration mediated by DOC has been shown to represent around a third of the North Atlantic CO_2 sink (Fontela et al., 2016). It has been demonstrated in DOC enrichment along the AMOC and its coupling with intense overturning in the NA SPSS leads to downward transport of 0.07 PgC yr^{-1} associated mainly with water masses transported by the DWBC (Fontela et al., 2020). In addition, 0.09 PgC yr^{-1} of DOC exported northward from the subtropics is mineralized in the deep layers of the AMOC. Inverse models do not include the DOC divergence, which is assumed to be small (Mikaloff Fletcher et al., 2007). This carbon cycle component has not been evaluated neither in RECCAP1 nor in RECCAP2, and considering the importance of its magnitude relative to FCO_2, it is relevant to consider it in future biogeochemical modeling experiments together with other modeling improvements proposed here. Articles highlighting the importance of DOC in the carbon balance are relatively recent (Fontela et al., 2016, 2020), with global non-seasonal climatology (Roshan & DeVries, 2017) and the compilation of a global DOC database (Hansell et al., 2021) being very recent, making it difficult to assess DOC modeling in GOBMs.

5. Conclusions

We provide here the current "best estimate" of surface CO_2 fluxes as well as the accumulation and transport of C_{ant} in the Atlantic, including the Mediterranean Sea for the RECCAP2 period, 1985–2018. For this estimate, we have compared different types of ocean biogeochemical models (GOBMs, ROBM, data-assimilated models) with various observation-based products. Our analysis includes several time-scales of variability.

We find that the *mean* net sea-air CO_2 flux of the GOBM ensemble is 27% stronger than estimates from observation-based pCO_2 products. This difference is within the uncertainties of the GOBMs and pCO_2 products and can be explained, in part, by known discrepancies between pCO_2 products and GOBMs. Specifically, this includes the oceanic CO_2 outgassing due to the impact of riverine discharge that is not explicitly represented in most GOBMs. The pCO_2 products may also be biased by not including near surface pCO_2 gradients. Adjusting for these effects mostly leads to higher fluxes into the ocean, which—if applied to all pCO_2 products—would lead to better agreement between GOBMs and pCO_2 products for the time period considered here.

The *trends* of sea-air CO_2 fluxes before and after the year 2000 are similar across our ensemble of GOBMs (from -0.045 ± 0.012 to -0.060 ± 0.017 PgC yr^{-1} dec^{-1}) and are consistent with the 43% increase in the atmospheric CO_2 growth rate between the pre-2000 period and the post-2000 periods. In contrast, the trends obtained from surface CO_2 observations show a sharp increase from the trend of the pre-2000 of -0.024 ± 0.075 PgC yr^{-1} dec^{-1} to a trend of -0.126 ± 0.031 PgC yr^{-1} dec^{-1} in the post-2000 period.

All biomes apart from the subpolar North Atlantic show a high correlation between GOBMs and pCO_2 products in terms of FCO_2 seasonality. In the North Atlantic subpolar biome, the GOBMs simulate a seasonal cycle driven predominantly by temperature variation, which the pCO_2 products do not show.

Averaged over the Atlantic, the ensemble of GOBMs shows lower interannual variability (IAV) in FCO_2 than the pCO_2 products. Spatially and temporally, IAV in pCO_2 products and GOBMs agree well in most of the Atlantic biomes but disagree quite substantially in the subpolar North Atlantic. Here, the variability of the GOBMs is mostly driven by SST variations, which is not the case for the pCO_2 products.

The mean C_{ant} storage change between 1994 and 2007 simulated by the GOBM ensemble was found to be 28% lower than that estimated from DIC observations in the ocean interior and 25% lower than the data-assimilated model. These differences are higher than the standard deviation of the GOBM estimates (17%). In contrast to the results described for the surface CO_2 fluxes, there is a high agreement in anthropogenic CO_2 storage rates between GOBMs and those based on DIC observations in the NA SPSS and NA STSS biomes, whereas there are significant differences in the NA STPS, AEQU, and SA STPS biomes, where the GOBM estimates are on average 36% lower than observation-based estimates. The GOBMs indicate that 32% of the C_{ant} accumulated in the Atlantic comes from the Southern Ocean, in line with previous estimates from the literature. The Mediterranean Sea revealed an almost balanced net sea-air flux of CO_2; however, it presented a C_{ant} accumulation of 0.018 PgC yr^{-1}, of which 70% are taken up from the atmosphere and 30% are imported from the Atlantic.

Estimates of the land-to-ocean transport of carbon and nutrients indicate a significant and large net CO_2 outgassing due to the input of this terrestrially derived matter. The protocol of RECCAP2 recommended the use of the updated estimate of 0.65 PgC yr^{-1} of Regnier et al. (2022) at the global level. For the Atlantic Ocean, the outgassing rates per square meter are twice the global rates when considering the spatial distribution of the riverine carbon outgassing (RCO) simulated by Lacroix et al. (2020). This RCO is especially significant in the NA STPS biome and hampers the comparison of GOBM and observation-based estimates of CO_2 fluxes, transport and accumulation. Therefore, it is essential to have more realistic models to better understand the influences of land-sea fluxes in the Atlantic Ocean and to be able to use observational-estimates with confidence when determining the accumulation of C_{ant}. This also requires better spatial and seasonal coverage of biogeochemical observations such as CO_2, nutrients and DOC to allow for improved model evaluation or even generate new emergent constraints.

Conflict of Interest

The authors declare no conflicts of interest relevant to this study.

Data Availability Statement

The RECCAP2 ocean data collection can be found in Müller (2023).

Acknowledgments

We are grateful for the formal reviewer comments and suggestions provided by Yuanxu Dong and the associated editors. F. F. Pérez and A. Velo were supported by the BOCATS2 (PID2019-104279GB-C21) project funded by MCIN/AEI/10.13039/501100011033 and by European Union under grant agreement no. 101094690 (EuroGO-SHIP), and with E. Huertas contributed to WATER:iOS CSIC PTI. M. Becker acknowledges funding from the Research Council of Norway through N-ICOS-2 (Grant 296012), and Nansen Legacy, Grant 276730. N. Goris was supported by the strategic project DYNASOR (DYnamics of the North Atlantic Surface and Overturning ciRculation) of the Bjerknes Centre for Climate Research. M. López-Mozos was supported by the Grant PRE2020-093138 funded by MCIN/AEI/10.13039/501100011033 and by "ESF Investing in your future." J. Tjiputra acknowledges funding from EU funded H2020 projects TRIATLAS (no. 817578) and OceanICU (no. 101083922). A. Olsen appreciates support from the Research Council of Norway through N-ICOS-2 (Grant 296012), and Horizon Europe through Grant 101083922 (OceanICU Improving Carbon Understanding). J.D. Müller and N. Gruber acknowledge support from the European Union's Horizon 2020 research and innovation program under grant agreement no. 821003 (project 4C) and no. 820989 (project COMFORT). M. Gehlen acknowledges support from the European Union's Horizon 2020 research and innovation program under grant agreements no. 820989 (project COMFORT) and no. 862923 (project AtlantECO), as well as from Horizon Europe through Grant 101083922 (OceanICU). T. Chau and M. Gehlen appreciate funding through the European Copernicus Marine Environment Monitoring Service (CMEMS) Grant 83-CMEMSTAC-MOB. J. Hauck acknowledges funding from the Initiative and Networking Fund of the Helmholtz Association (Helmholtz Young Investigator Group Marine Carbon and Ecosystem feedback in the Earth System [MarESys], Grant VH-NG-1301) and from ERC-2022-STG OceanPeak, Grant agreement 101077209. R. Wanninkof acknowledges funding from the NOAA/OAR Global Ocean Monitoring and Observation Program (GOMO).

References

Álvarez, M., Ríos, A. F., Pérez, F. F., Bryden, H. L., & Rosón, G. (2003). Transports and budgets of total inorganic carbon in the subpolar and temperate North Atlantic. *Global Biogeochemical Cycles*, *17*(1), 2-1–2-21. https://doi.org/10.1029/2002GB001881

Aumont, O., Ethe, C., Tagliabue, A., Bopp, L., & Gehlen, M. (2015). PISCES-v2: An ocean biogeochemical model for carbon and ecosystem studies. *Geoscientific Model Development*, *8*, 2465–2513. https://doi.org/10.5194/gmd-8-2465-2015

Aumont, O., Orr, J. C., Monfray, P., Ludwig, W., Amiotte-Suchet, P., & Probst, J.-L. (2001). Riverine-driven interhemispheric transport of carbon. *Global Biogeochemical Cycles*, *15*(2), 393–405. https://doi.org/10.1029/1999GB001238

Bakker, D. C. E., Alin, S. R., Becker, M., Bittig, H., Castaño-Primo, R., Feely, R. A., et al. (2022). SOCAT version 2022 for quantification of ocean CO_2 uptake. Retrieved from https://www.socat.info/wp-content/uploads/2022/06/2022_Poster_SOCATv2022_release.pdf

Bakker, D. C. E., Pfeil, B., Landa, C. S., Metzl, N., O'Brien, K. M., Olsen, A., et al. (2016). A multi-decade record of high-quality CO_2 data in version 3 of the surface ocean CO_2 Atlas (SOCAT). *Earth System Science Data*, *8*(2), 383–413. https://doi.org/10.5194/essd-8-383-2016

Bates, N. R., Astor, Y. M., Church, M. J., Currie, K., Dore, J. E., González-Dávila, M., et al. (2014). A time-series view of changing surface ocean chemistry due to ocean uptake of anthropogenic CO_2 and ocean acidification. *Oceanography*, *27*(1), 126–141. https://doi.org/10.5670/oceanog.2014.16

Bates, N. R., Takahashi, T., Chipman, D. W., & Knap, A. H. (1998). Variability of pCO_2 on diel to seasonal timescales in the Sargasso Sea near Bermuda. *Journal of Geophysical Research*, *103*(C8), 15567–15585. https://doi.org/10.1029/98JC00247

Becker, M., Steinhoff, T., & Körtzinger, A. (2018). A detailed view on the seasonality of stable carbon isotopes across the North Atlantic. *Global Biogeochemical Cycles*, *32*(9), 1406–1419. https://doi.org/10.1029/2018GB005905

Bellenger, H., Bopp, L., Ethé, C., Ho, D., Duvel, J. P., Flavoni, S., et al. (2023). Sensitivity of the global ocean carbon sink to the ocean skin in a climate model. *Journal of Geophysical Research: Oceans*, *128*(7), 1–22. https://doi.org/10.1029/2022JC019479

Blomquist, B. W., Brumer, S. E., Fairall, C. W., Huebert, B. J., Zappa, C. J., Brooks, I. M., et al. (2017). Wind speed and sea state dependencies of air-sea gas transfer: Results from the high wind speed gas exchange study (HiWinGS). *Journal of Geophysical Research: Oceans*, *122*(10), 8034–8062. https://doi.org/10.1002/2017JC013181

Bower, A., Lozier, S., Biastoch, A., Drouin, K., Foukal, N., Furey, H., et al. (2019). Lagrangian views of the pathways of the Atlantic meridional overturning circulation. *Journal of Geophysical Research: Oceans*, *124*(8), 5313–5335. https://doi.org/10.1029/2019JC015014

Brady, R. X., Lovenduski, N. S., Alexander, M. A., Jacox, M., & Gruber, N. (2019). On the role of climate modes in modulating the air–sea CO_2 fluxes in eastern boundary upwelling systems. *Biogeosciences*, *16*(2), 329–346. https://doi.org/10.5194/bg-16-329-2019

Breeden, M. L., & McKinley, G. A. (2016). Climate impacts on multidecadal pCO_2 variability in the North Atlantic: 1948–2009. *Biogeosciences*, *13*(11), 3387–3396. https://doi.org/10.5194/bg-13-3387-2016

Brown, P. J., McDonagh, E. L., Sanders, R., Watson, A. J., Wanninkhof, R., King, B. A., et al. (2021). Circulation-driven variability of Atlantic anthropogenic carbon transports and uptake. *Nature Geoscience*, *14*(8), 571–577. https://doi.org/10.1038/s41561-021-00774-5

Butterworth, B. J., & Miller, S. D. (2016). Air-sea exchange of carbon dioxide in the Southern Ocean and Antarctic marginal ice zone. *Geophysical Research Letters*, *43*(13), 7223–7230. https://doi.org/10.1002/2016GL069581

Caínzos, V., Velo, A., Pérez, F. F., & Hernández-Guerra, A. (2022). Anthropogenic carbon transport variability in the Atlantic Ocean over three decades. *Global Biogeochemical Cycles*, *36*(11), e2022GB007475. https://doi.org/10.1029/2022GB007475

Chassignet, E. P., Yeager, S. G., Fox-Kemper, B., Bozec, A., Castruccio, F., Danabasoglu, G., et al. (2020). Impact of horizontal resolution on global ocean–sea ice model simulations based on the experimental protocols of the Ocean Model Intercomparison Project phase 2 (OMIP-2). *Geoscientific Model Development*, *13*(9), 4595–4637. https://doi.org/10.5194/gmd-13-4595-2020

Chau, T. T. T., Gehlen, M., & Chevallier, F. (2022). A seamless ensemble-based reconstruction of surface ocean pCO_2 and air–sea CO_2 fluxes over the global coastal and open oceans. *Biogeosciences*, *19*(4), 1087–1109. https://doi.org/10.5194/bg-19-1087-2022

Clement, D., & Gruber, N. (2018). The eMLR (C*) method to determine decadal changes in the global ocean storage of anthropogenic CO_2. *Global Biogeochemical Cycles*, *32*(4), 654–679. https://doi.org/10.1002/2017GB005819

Coppola, L., Diamond Riquier, E., & Carval, T. (2018). *Dyfamed observatory data*. SEANOE. https://doi.org/10.17882/43749

De Carlo, E. H., Mousseau, L., Passafiume, O., Drupp, P. S., & Gattuso, J.-P. (2013). Carbonate chemistry and air–sea CO_2 flux in a NW Mediterranean Bay over a four-year period: 2007–2011. *Aquatic Geochemistry*, *19*(5–6), 399–442. https://doi.org/10.1007/s10498-013-9217-4

Denvil-Sommer, A., Gehlen, M., Vrac, M., & Mejia, C. (2019). LSCE-FFNN-v1: A two-step neural network model for the reconstruction of surface ocean pCO_2 over the global ocean. *Geoscientific Model Development*, *12*(5), 2091–2105. https://doi.org/10.5194/gmd-12-2091-2019

DeVries, T. (2022). Atmospheric CO_2 and sea surface temperature variability cannot explain recent decadal variability of the ocean CO_2 sink. *Geophysical Research Letters*, *49*(7), e2021GL096018. https://doi.org/10.1029/2021GL096018

DeVries, T., Yamamoto, K., Wanninkhof, R., Gruber, N., Hauck, J., Müller, J. D., et al. (2023). Magnitude, trends, and variability of the global ocean carbon sink from 1985-2018. *Global Biogeochemical Cycles*, *37*(10), e2023GB007780. https://doi.org/10.1029/2023GB007780

Doney, S. C., Lindsay, K., Caldeira, K., Campin, J.-M., Drange, H., Dutay, J.-C., et al. (2004). Evaluating global ocean carbon models: The importance of realistic physics. *Global Biogeochemical Cycles*, *18*(3), GB3017. https://doi.org/10.1029/2003GB002150

Dong, Y., Bakker, D. C. E., Bell, T. G., Huang, B., Landschützer, P., Liss, P. S., & Yang, M. (2022). Update on the temperature corrections of global air-sea CO_2 flux estimates. *Global Biogeochemical Cycles*, *36*(9), e2022GB007360. https://doi.org/10.1029/2022GB007360

Fajar, N. M., Guallart, E. F., Steinfeldt, R., Ríos, A. F., Pelegrí, J. L., Pelejero, C., et al. (2015). Anthropogenic CO_2 changes in the equatorial Atlantic Ocean. *Progress in Oceanography*, *134*, 256–270. https://doi.org/10.1016/j.pocean.2015.02.004

Fay, A. R., & McKinley, G. A. (2014). Global open-ocean biomes: Mean and temporal variability. *Earth System Science Data*, *6*(2), 273–284. https://doi.org/10.5194/essd-6-273-2014

Fernández-Castro, B., Álvarez, M., Nieto-Cid, M., Zunino, P., Mercier, H., & Álvarez-Salgado, X. A. (2019). Dissolved organic nitrogen production and export by meridional overturning in the eastern subpolar North Atlantic. *Geophysical Research Letters*, *46*(7), 3832–3842. https://doi.org/10.1029/2018GL080284

Fontela, M., García-Ibáñez, M. I., Hansell, D. A., Mercier, H., & Pérez, F. F. (2016). Dissolved organic carbon in the North Atlantic meridional overturning circulation. *Scientific Reports*, *6*(1), 26931. https://doi.org/10.1038/srep26931

Fontela, M., Pérez, F. F., Mercier, H., & Lherminier, P. (2020). North Atlantic western boundary currents are intense dissolved organic carbon streams. *Frontiers in Marine Science*, *7*, 593757. https://doi.org/10.3389/fmars.2020.593757

Friedlingstein, P., Jones, M. W., O'Sullivan, M., Andrew, R. M., Bakker, D. C. E., Hauck, J., et al. (2022). Global carbon budget 2021. *Earth System Science Data*, *14*(4), 1917–2005. https://doi.org/10.5194/essd-14-1917-2022

Fröb, F., Olsen, A., Becker, M., Chafik, L., Johannessen, T., Reverdin, G., & Omar, A. (2019). Wintertime fCO_2 variability in the subpolar North Atlantic since 2004. *Geophysical Research Letters*, *46*(3), 1580–1590. https://doi.org/10.1029/2018gl080554

Fröb, F., Olsen, A., Våge, K., Moore, K., Yashayaev, I., Jeansson, E., & Rajasakaren, B. (2016). Irminger Sea deep convection injects oxygen and anthropogenic carbon to the ocean interior. *Nature Communications*, *7*(1), 13244. https://doi.org/10.1038/ncomms13244

Gao, S., Schwinger, J., Tjiputra, J., Bethke, I., Hartmann, J., Mayorga, E., & Heinze, C. (2023). Riverine impact on future projections of marine primary production and carbon uptake. *Biogeosciences*, *20*(1), 93–119. https://doi.org/10.5194/bg-20-93-2023

Gehlen, M., Barciela, R., Bertino, L., Brasseur, P., Butenschön, M., Chai, F., et al. (2015). Building the capacity for forecasting marine biogeochemistry and ecosystems: Recent advances and future developments. *Journal of Operational Oceanography*, *8*(1), s168–s187. https://doi.org/10.1080/1755876X.2015.1022350

Gerber, M., Joos, F., Vázquez-Rodríguez, M., Touratier, F., & Goyet, C. (2009). Regional air-sea fluxes of anthropogenic carbon inferred with an Ensemble Kalman Filter. *Global Biogeochemical Cycles*, *23*(1). https://doi.org/10.1029/2008GB003247

Gharamti, M., Tjiputra, J., Bethke, I., Samuelsen, A., Skjelvan, I., Bentsen, M., & Bertino, L. (2017). Ensemble data assimilation for ocean biogeochemical state and parameter estimation at different sites. *Ocean Modelling*, *112*, 65–89. https://doi.org/10.1016/j.ocemod.2017.02.006

Gloege, L., McKinley, G. A., Landschützer, P., Fay, A. R., Frölicher, T. L., Fyfe, J. C., et al. (2021). Quantifying errors in observationally based estimates of ocean carbon sink variability. *Global Biogeochemical Cycles*, *35*(4), e2020GB006788. https://doi.org/10.1029/2020GB006788

Goddijn-Murphy, L. M., Woolf, D. K., Land, P. E., Shutler, J. D., & Donlon, C. (2015). The OceanFlux Greenhouse Gases methodology for deriving a sea surface climatology of CO_2 fugacity in support of air–sea gas flux studies. *Ocean Science*, *11*(4), 519–541. https://doi.org/10.5194/os-11-519-2015

González-Dávila, M., Santana-Casiano, J. M., Rueda, M. J., & Llinás, O. (2010). The water column distribution of carbonate system variables at the ESTOC site from 1995 to 2004. *Biogeosciences*, *7*(10), 3067–3081. https://doi.org/10.5194/bg-7-3067-2010

Gonzalez-Dávila, M., Santana Casiano, J. M., & Ucha, I. R. (2009). Seasonal variability of fCO_2 in the Angola-Benguela region. *Progress in Oceanography*, *83*(1–4), 124–133. https://doi.org/10.1016/j.pocean.2009.07.033

Goris, N., Johannsen, K., & Tjiputra, J. (2023). The emergence of the Gulf Stream and interior western boundary as key regions to constrain the future North Atlantic carbon uptake. *Geoscientific Model Development*, *16*(8), 2095–2117. https://doi.org/10.5194/gmd-16-2095-2023

Goris, N., Tjiputra, J., Schwinger, J., & Heinze, C. (2015). Responses of carbon uptake and oceanic pCO_2 to climate change in the North Atlantic: A model study with the Bergen Earth system model. *Global Biogeochemical Cycles*, *29*(10), 1567–1583. https://doi.org/10.1002/2015GB005109

Goris, N., Tjiputra, J. F., Olsen, A., Schwinger, J., Lauvset, S. K., & Jeansson, E. (2018). Constraining projection-based estimates of the future North Atlantic carbon uptake. *Journal of Climate*, *31*(10), 3959–3978. https://doi.org/10.1175/JCLI-D-17-0564.1

Gregor, L., & Gruber, N. (2021). OceanSODA-ETHZ: A global gridded data set of the surface ocean carbonate system for seasonal to decadal studies of ocean acidification. *Earth System Science Data*, *13*(2), 777–808. https://doi.org/10.5194/essd-13-777-2021

Gregor, L., Lebehot, A. D., Kok, S., & Scheel Monteiro, P. M. (2019). A comparative assessment of the uncertainties of global surface ocean CO_2 estimates using a machine-learning ensemble (CSIR-ML6 version 2019a)–have we hit the wall? *Geoscientific Model Development*, *12*(12), 5113–5136. https://doi.org/10.5194/gmd-12-5113-2019

Gruber, N., Clement, D., Carter, B. R., Feely, R. A., van Heuven, S., Hoppema, M., et al. (2019). The oceanic sink for anthropogenic CO_2 from 1994 to 2007. *Science*, *363*(6432), 1193–1199. https://doi.org/10.1126/science.aau5153

Gruber, N., Gloor, M., Mikaloff Fletcher, S. E., Doney, S. C., Dutkiewicz, S., Follows, M. J., et al. (2009). Oceanic sources, sinks, and transport of atmospheric CO_2. *Global Biogeochemical Cycles*, *23*(1), GB1005. https://doi.org/10.1029/2008GB003349

Gruber, N., Keeling, C. D., & Bates, N. R. (2002). Interannual variability in the North Atlantic Ocean carbon sink. *Science*, *298*(5602), 2374–2378. https://doi.org/10.1126/science.1077077

Gruber, N., Keeling, C. D., & Stocker, T. F. (1998). Carbon-13 constraints on the seasonal inorganic carbon budget at the BATS site in the northwestern Sargasso Sea. *Deep Sea Research Part I: Oceanographic Research Papers*, *45*(4–5), 673–717. https://doi.org/10.1016/S0967-0637(97)00098-8

Haine, T. W. N. (2016). Vagaries of Atlantic overturning. *Nature Geoscience*, *9*(7), 479–480. https://doi.org/10.1038/ngeo2748

Hansell, D. A. (2013). Recalcitrant dissolved organic carbon fractions. *Annual Review of Marine Science*, *5*(1), 421–445. https://doi.org/10.1146/annurev-marine-120710-100757

Hansell, D. A., Carlson, C. A., Amon, R. M. W., Álvarez-Salgado, X. A., Yamashita, Y., Romera-Castillo, C., & Bif, M. B. (2021). Compilation of dissolved organic matter (DOM) data obtained from the global ocean surveys from 1994 to 2021 (NCEI Accession 0227166) [Dataset]. *NOAA National Centers for Environmental Information*. https://doi.org/10.25921/s4f4-ye35

Hassoun, A. E. R., Gemayel, E., Krasakopoulou, E., Goyet, C., Saab, M. A.-A., Guglielmi, V., et al. (2015). Acidification of the Mediterranean Sea from anthropogenic carbon penetration. *Deep Sea Research Part I: Oceanographic Research Papers*, *102*, 1–15. https://doi.org/10.1016/j.dsr.2015.04.005

Hauck, J., Gregor, L., Nissen, C., Patara, L., Hague, M., Mongwe, N. P., et al. (2023). The Southern Ocean carbon cycle 1985-2018: Mean, seasonal cycle, trends and storage. *Global Biogeochemical Cycles*, *37*(11), e2023GB007848. https://doi.org/10.1029/2023GB007848

Hauck, J., Nissen, C., Landschützer, P., Rödenbeck, C., Bushinsky, S., & Olsen, A. (2023). Sparse observations induce large biases in estimates of the global ocean CO_2 sink: An ocean model subsampling experiment. *Philosophical Transactions of the Royal Society*, *381*(2249), 20220063. https://doi.org/10.1098/rsta.2022.0063

Hauck, J., & Völker, C. (2015). Rising atmospheric CO_2 leads to large impact of biology on Southern Ocean CO_2 uptake via changes of the Revelle factor. *Geophysical Research Letters*, *42*(5), 1459–1464. https://doi.org/10.1002/2015GL063070

Hauck, J., Zeising, M., Le Quéré, C., Gruber, N., Bakker, D. C. E., Bopp, L., et al. (2020). Consistency and challenges in the ocean carbon sink estimate for the global carbon budget. *Frontiers in Marine Science*, *7*, 1–22. https://doi.org/10.3389/fmars.2020.571720

Hirschi, J. J.-M., Barnier, B., Böning, C., Biastoch, A., Blaker, A. T., Coward, A., et al. (2020). The Atlantic meridional overturning circulation in high-resolution models. *Journal of Geophysical Research: Oceans*, *125*(4), e2019JC015522. https://doi.org/10.1029/2019JC015522

Ho, D. T., Law, C. S., Smith, M. J., Schlosser, P., Harvey, M., & Hill, P. (2006). Measurements of air-sea gas exchange at high wind speeds in the Southern Ocean: Implications for global parameterizations. *Geophysical Research Letters*, *33*(16), L16611. https://doi.org/10.1029/2006GL026817

Holfort, J., Johnson, K. M., Schneider, B., Siedler, G., & Wallace, D. W. (1998). Meridional transport of dissolved inorganic carbon in the South Atlantic Ocean. *Global Biogeochemical Cycles*, *12*(3), 479–499. https://doi.org/10.1029/98GB01533

Huertas, I. E., Ríos, A. F., García-Lafuente, J., Makaoui, A., Rodríguez-Gálvez, S., Sánchez-Román, A., et al. (2009). Anthropogenic and natural CO_2 exchange through the Strait of Gibraltar. *Biogeosciences*, *6*(4), 647–662. https://doi.org/10.5194/bg-6-647-2009

Iida, Y., Kojima, A., Takatani, Y., & Ishii, M. (2021). Global trends of ocean CO_2 sink and ocean acidification: An observation-based reconstruction of surface ocean inorganic carbon variables. *Journal of Oceanography*, *77*(2), 323–358. https://doi.org/10.1007/s10872-020-00571-5

Ingrosso, G., Giani, M., Comici, C., Kralj, M., Piacentino, S., De Vittor, C., & Del Negro, P. (2016). Drivers of the carbonate system seasonal variations in a Mediterranean gulf. *Estuarine, Coastal and Shelf Science*, *168*, 58–70. https://doi.org/10.1016/j.ecss.2015.11.001

Ito, R. G., Schneider, B., & Thomas, H. (2005). Distribution of surface fCO_2 and air-sea fluxes in the southwestern subtropical Atlantic and adjacent continental shelf. *Journal of Marine Systems*, *56*(3–4), 227–242. https://doi.org/10.1016/j.jmarsys.2005.02.005

Jacobson, A. R., Mikaloff Fletcher, S. E., Gruber, N., Sarmiento, J. L., & Gloor, M. (2007). A joint atmosphere-ocean inversion for surface fluxes of carbon dioxide: 2. Regional results. *Global Biogeochemical Cycles*, *21*(1). https://doi.org/10.1029/2006GB002703

Jeansson, E., Olsen, A., Eldevik, T., Skjelvan, I., Omar, A. M., Lauvset, S. K., et al. (2011). The Nordic Seascarbon budget: Sources, sinks, and uncertainties. *Global Biogeochemical Cycles*, *25*(4), GB4010. https://doi.org/10.1029/2010GB003961

Jing, Y., Li, Y., Xu, Y., & Fan, G. (2019). Influences of the NAO on the North Atlantic CO_2 fluxes in winter and summer on the interannual scale. *Advances in Atmospheric Sciences*, *36*(11), 1288–1298. https://doi.org/10.1007/s00376-019-8247-2

Kapsenberg, L., Alliouane, S., Gazeau, F., Mousseau, L., & Gattuso, J.-P. (2017). Coastal ocean acidification and increasing total alkalinity in the northwestern Mediterranean Sea. *Ocean Science*, *13*(3), 411–426. https://doi.org/10.5194/os-13-411-2017

Keeling, C. D. (1993). Lecture 2: Surface ocean CO_2. In *The global carbon cycle* (pp. 413–429). Springer Berlin Heidelberg. https://doi.org/10.1007/978-3-642-84608-3_17

Keeling, R. F., & Peng, T.-H. (1995). Transport of heat, CO_2 and O_2 by the Atlantic's thermohaline circulation. *Philosophical Transactions of the Royal Society of London - B*, *348*, 133–142. https://doi.org/10.1098/rstb.1995.0055

Khatiwala, S., Primeau, F., & Hall, T. (2009). Reconstruction of the history of anthropogenic CO_2 concentrations in the ocean. *Nature*, *462*(7271), 346–349. https://doi.org/10.1038/nature08526

Khatiwala, S., Tanhua, T., Mikaloff Fletcher, S., Gerber, M., Doney, S. C., Graven, H. D., et al. (2013). Global ocean storage of anthropogenic carbon. *Biogeosciences*, *10*(4), 2169–2191. https://doi.org/10.5194/bg-10-2169-2013

Koseki, S., Tjiputra, J., Fransner, F., Crespo, L. R., & Keenlyside, N. S. (2023). Disentangling the impact of Atlantic Niño on sea-air CO_2 flux. *Nature Communications*, *14*(1), 3649. https://doi.org/10.1038/s41467-023-38718-9

Krasakopoulou, E., Rapsomanikis, S., Papadopoulos, A., & Papathanassiou, E. (2009). Partial pressure and air-sea CO_2 flux in the Aegean Sea during February 2006. *Continental Shelf Research*, *29*(11–12), 1477–1488. https://doi.org/10.1016/j.csr.2009.03.015

Krasakopoulou, E., Souvermezoglou, E., & Goyet, C. (2017). Carbonate system parameters and anthropogenic CO_2 in the North Aegean Sea during October 2013. *Continental Shelf Research*, *149*, 69–81. https://doi.org/10.1016/j.csr.2017.04.002

Lacroix, F., Ilyina, T., & Hartmann, J. (2020). Oceanic CO_2 outgassing and biological production hotspots induced by pre-industrial river loads of nutrients and carbon in a global modeling approach. *Biogeosciences*, *17*(1), 55–88. https://doi.org/10.5194/bg-17-55-2020

Landschützer, P., Gruber, N., E. Bakker, D. C., & Schuster, U. (2014). Recent variability of the global ocean carbon sink. *Global Biogeochemical Cycles*, *28*(9), 927–949. https://doi.org/10.1002/2014GB004853

Leseurre, C., Lo Monaco, C., Reverdin, G., Metzl, N., Fin, J., Olafsdottir, S., & Racapé, V. (2020). Ocean carbonate system variability in the North Atlantic subpolar surface water (1993–2017). *Biogeosciences*, *17*(9), 2553–2577. https://doi.org/10.5194/bg-17-2553-2020

Louchard, D., Gruber, N., & Münnich, M. (2021). The impact of the Amazon on the biological pump and the air-sea CO_2 balance of the western tropical Atlantic. *Global Biogeochemical Cycles*, *35*(6). https://doi.org/10.1029/2020GB006818

Ma, X., Jing, Z., Chang, P., Liu, X., Montuoro, R., Small, R. J., et al. (2016). Western boundary currents regulated by interaction between ocean eddies and the atmosphere. *Nature*, *535*(7613), 533–537. https://doi.org/10.1038/nature18640

Macdonald, A. M., Baringer, M. O., Wanninkhof, R., Lee, K., & Wallace, D. W. R. (2003). A 1998_1992 comparison of inorganic carbon and its transport across 24.5°N in the Atlantic. *Deep Sea Research Part II: Topical Studies in Oceanography*, *50*(22–26), 3041–3064. https://doi.org/10.1016/j.dsr2.2003.07.009

Macovei, V. A., Hartman, S. E., Schuster, U., Torres-Valdés, S., Moore, C. M., & Sanders, R. J. (2020). Impact of physical and biological processes on temporal variations of the ocean carbon sink in the mid-latitude North Atlantic (2002–2016). *Progress in Oceanography*, *180*, 102223. https://doi.org/10.1016/j.pocean.2019.102223

McKinley, G. A., Fay, A. R., Eddebbar, Y. A., Gloege, L., & Lovenduski, N. S. (2020). External forcing explains recent decadal variability of the ocean carbon sink. *AGU Advances*, *1*(2), e2019AV000149. https://doi.org/10.1029/2019AV000149

McKinley, G. A., Fay, A. R., Takahashi, T., & Metzl, N. (2011). Convergence of atmospheric and North Atlantic carbon dioxide trends on multidecadal timescales. *Nature Geoscience*, *4*(9), 606–610. https://doi.org/10.1038/ngeo1193

McKinley, G. A., Ritzer, A. L., & Lovenduski, N. S. (2018). Mechanisms of northern North Atlantic biomass variability. *Biogeosciences*, *15*(20), 6049–6066. https://doi.org/10.5194/bg-15-6049-2018

Michaels, A. F., Bates, N. R., Buesseler, K. O., Carlson, C. A., & Knap, A. H. (1994). Carbon-cycle imbalances in the Sargasso Sea. *Nature*, *372*(6506), 537–540. https://doi.org/10.1038/372537a0

Mikaloff Fletcher, S. E., Gruber, N., Jacobson, A. R., Doney, S. C., Dutkiewicz, S., Gerber, M., et al. (2006). Inverse estimates of anthropogenic CO_2 uptake, transport, and storage by the ocean. *Global Biogeochemical Cycles*, *20*(2), GB2002. https://doi.org/10.1029/2005GB002530

Mikaloff Fletcher, S. E., Gruber, N., Jacobson, A. R., Gloor, M., Doney, S. C., Dutkiewicz, S., et al. (2007). Inverse estimates of the oceanic sources and sinks of natural CO_2 and the implied oceanic carbon transport. *Global Biogeochemical Cycles*, *21*(1), GB1010. https://doi.org/10.1029/2006GB002751

Müller, J. D. (2023). RECCAP2-ocean data collection [Dataset]. *Zenodo*. https://doi.org/10.5281/zenodo.7990823

Müller, J. D., Gruber, N., Carter, B., Feely, R., Ishii, M., Lange, N., et al. (2023). Decadal trends in the oceanic storage of anthropogenic carbon from 1994 to 2014. *AGU Advances*, *4*, e2023AV000875. https://doi.org/10.1029/2023AV000875

Nightingale, P. D., Malin, G., Law, C. S., Watson, A. J., Liss, P. S., Liddicoat, M. I., et al. (2000). In situ evaluation of air-sea gas exchange parameterizations using novel conservative and volatile tracers. *Global Biogeochemical Cycles*, *14*(1), 373–387. https://doi.org/10.1029/1999GB900091

Olsen, A., Brown, K. R., Chierici, M., Johannessen, T., & Neill, C. (2008). Sea-surface CO_2 fugacity in the subpolar North Atlantic. *Biogeosciences*, *5*(2), 535–547. https://doi.org/10.5194/bg-5-535-2008

Olsen, A., Key, R. M., Van Heuven, S., Lauvset, S. K., Velo, A., Lin, X., et al. (2016). The Global Ocean Data Analysis Project version 2 (GLODAPv2)–an internally consistent data product for the world ocean. *Earth System Science Data*, *8*(2), 297–323. https://doi.org/10.5194/essd-8-297-2016

Padin, X. A., Vazquez-Rodrıguez, M., Castaño, M., Velo, A., Alonso-Perez, F., Gago, J., et al. (2010). Air-sea CO_2 fluxes in the Atlantic as measured during boreal spring and autumn. *Biogeosciences*, *7*(5), 1587–1606. https://doi.org/10.5194/bg-7-1587-2010

Park, G.-H., Wanninkhof, R., Doney, S. C., Takahashi, T., Lee, K., Feely, R. A., et al. (2010). Variability of global net sea–air CO_2 fluxes over the last three decades using empirical relationships. *Tellus B: Chemical and Physical Meteorology*, *62*(5), 352–368. https://doi.org/10.1111/j.1600-0889.2010.00498.x

Pérez, F. F., Mercier, H., Vázquez-Rodríguez, M., Lherminier, P., Velo, A., Pardo, P. C., et al. (2013). Atlantic Ocean CO_2 uptake reduced by weakening of the meridional overturning circulation. *Nature Geoscience*, *6*(2), 146–152. https://doi.org/10.1038/ngeo1680

Pérez, F. F., Vázquez-Rodríguez, M., Louarn, E., Padín, X. A., Mercier, H., & Ríos, A. F. (2008). Temporal variability of the anthropogenic CO_2 storage in the Irminger Sea. *Biogeosciences*, *5*(6), 1669–1679. https://doi.org/10.5194/bg-5-1669-2008

Petihakis, G., Perivoliotis, L., Korres, G., Ballas, D., Frangoulis, C., Pagonis, P., et al. (2018). An integrated open-coastal biogeochemistry, ecosystem and biodiversity observatory of the eastern Mediterranean–the Cretan Sea component of the POSEIDON system. *Ocean Science*, *14*(5), 1223–1245. https://doi.org/10.5194/os-14-1223-2018

Pfeil, B., Olsen, A., Bakker, D. C. E., Hankin, S., Koyuk, H., Kozyr, A., et al. (2013). A uniform, quality controlled surface ocean CO_2 atlas (SOCAT). *Earth System Science Data*, *5*(1), 125–143. https://doi.org/10.5194/essd-5-125-2013

Racapé, V., Zunino, P., Mercier, H., Lherminier, P., Bopp, L., Pérez, F. F., & Gehlen, M. (2018). Transport and storage of anthropogenic C in the North Atlantic subpolar ocean. *Biogeosciences*, *15*(14), 4661–4682. https://doi.org/10.5194/bg-15-4661-2018

Regnier, P., Friedlingstein, P., Ciais, P., Mackenzie, F. T., Gruber, N., Janssens, I. A., et al. (2013). Anthropogenic perturbation of the carbon fluxes from land to ocean. *Nature Geoscience*, *6*(8), 597–607. https://doi.org/10.1038/ngeo1830

Regnier, P., Resplandy, L., Najjar, R. G., & Ciais, P. (2022). The land-to-ocean loops of the global carbon cycle. *Nature*, *603*(7901), 401–410. https://doi.org/10.1038/s41586-021-04339-9

Resplandy, L., Keeling, R. F., Rödenbeck, C., Stephens, B. B., Khatiwala, S., Rodgers, K. B., et al. (2018). Revision of global carbon fluxes based on a reassessment of oceanic and riverine carbon transport. *Nature Geoscience*, *11*(7), 504–509. https://doi.org/10.1038/s41561-018-0151-3

Rhein, M., Kieke, D., & Steinfeldt, R. (2015). Advection of North Atlantic deep water from the Labrador Sea to the southern hemisphere. *Journal of Geophysical Research: Oceans*, *120*(4), 2471–2487. https://doi.org/10.1002/2014JC010605

Rhein, M., Steinfeldt, R., Kieke, D., Stendardo, I., & Yashayaev, I. (2017). Ventilation variability of Labrador Sea Water and its impact on oxygen and anthropogenic carbon: A review. *Philosophical Transactions A*, *375*(2102), 20160321. https://doi.org/10.1098/rsta.2016.0321

Ríos, A. F., Álvarez-Salgado, X. A., Pérez, F. F., Bingler, L. S., Arístegui, J., & Mémery, L. (2003). Carbon dioxide along WOCE line A14: Water masses characterization and anthropogenic entry. *Journal of Geophysical Research*, *108*(C4), 3123. https://doi.org/10.1029/2000JC000366

Ríos, A. F., Velo, A., Pardo, P. C., Hoppema, M., & Pérez, F. F. (2012). An update of anthropogenic CO_2 storage rates in the western South Atlantic basin and the role of Antarctic Bottom Water. *Journal of Marine Systems*, *94*, 197–203. https://doi.org/10.1016/j.jmarsys.2011.11.023

Rödenbeck, C., Bakker, D. C., Metzl, N., Olsen, A., Sabine, C., Cassar, N., et al. (2014). Interannual sea–air CO_2 flux variability from an observation-driven ocean mixed-layer scheme. *Biogeosciences*, *11*(17), 4599–4613. https://doi.org/10.5194/bg-11-4599-2014

Rödenbeck, C., Bakker, D. C. E., Gruber, N., Iida, Y., Jacobson, A. R., Jones, S., et al. (2015). Data-based estimates of the ocean carbon sink variability—First results of the Surface Ocean pCO_2 Mapping intercomparison (SOCOM). *Biogeosciences*, *12*(23), 7251–7278. https://doi.org/10.5194/bg-12-7251-2015

Rödenbeck, C., Keeling, R. F., Bakker, D. C. E., Metzl, N., Olsen, A., Sabine, C., & Heimann, M. (2013). Global surface-ocean pCO_2 and sea–air CO_2 flux variability from an observation-driven ocean mixed-layer scheme. *Ocean Science*, *9*(2), 193–216. https://doi.org/10.5194/os-9-193-2013

Rodgers, K. B., Schwinger, J., Fassbender, A. J., Landschützer, P., Yamaguchi, R., Frenzel, H., et al. (2023). Seasonal variability of the surface ocean carbon cycle: A synthesis. *Global Biogeochemical Cycles*, *37*(9), e2023GB007798. https://doi.org/10.1029/2023GB007798

Roshan, S., & DeVries, T. (2017). Efficient dissolved organic carbon production and export in the oligotrophic ocean. *Nature Communications*, *8*(1), 2036. https://doi.org/10.1038/s41467-017-02227-3

Rosón, G., Ríos, A. F., Pérez, F. F., Lavín, A., & Bryden, H. L. (2003). Carbon distribution, fluxes, and budgets in the subtropical North Atlantic Ocean (24.5N). *Journal of Geophysical Research*, *108*(C5), 3144. https://doi.org/10.1029/1999jc000047

Sabine, C. L., Feely, R. A., Gruber, N., Key, R. M., Lee, K., Bullister, J. L., et al. (2004). The oceanic sink for anthropogenic CO_2. *Science*, *305*(5682), 367–371. https://doi.org/10.1126/science.1097403

Sabine, C. L., Hankin, S., Koyuk, H., Bakker, D. C. E., Pfeil, B., Olsen, A., et al. (2013). Surface ocean CO_2 Atlas (SOCAT) gridded data products. *Earth System Science Data*, *5*(1), 145–153. https://doi.org/10.5194/essd-5-145-2013

Santana-Casiano, J. M., González-Dávila, M., Rueda, M., Llinás, O., & González-Dávila, E.-F. (2007). The interannual variability of oceanic CO_2 parameters in the northeast Atlantic subtropical gyre at the ESTOC site. *Global Biogeochemical Cycles*, *21*(1), GB1015. https://doi.org/10.1029/2006GB002788

Santana-Casiano, J. M., González-Dávila, M., & Ucha, I. R. (2009). Carbon dioxide fluxes in the Benguela upwelling system during winter and spring: A comparison between 2005 and 2006. *Deep Sea Research Part II: Topical Studies in Oceanography*, *56*(8–10), 533–541. https://doi.org/10.1016/j.dsr2.2008.12.010

Sarmiento, J. L., & Gruber, N. (2006). *Ocean biogeochemical dynamics*. Princeton University Press.

Sarmiento, J. L., & Sundquist, E. T. (1992). Revised budget for the oceanic uptake of anthropogenic carbon dioxide. *Nature*, *356*(6370), 589–593. https://doi.org/10.1038/356589a0

Schneider, A., Tanhua, T., Körtzinger, A., & Wallace, D. W. (2010). High anthropogenic carbon content in the eastern Mediterranean. *Journal of Geophysical Research*, *115*(C12), C12050. https://doi.org/10.1029/2010JC006171

Schuster, U., McKinley, G. A., Bates, N., Chevallier, F., Doney, S. C., Fay, A. R., et al. (2013). An assessment of the Atlantic and Arctic sea–air CO_2 fluxes, 1990–2009. *Biogeosciences*, *10*(1), 607–627. https://doi.org/10.5194/bg-10-607-2013

Schwinger, J., Goris, N., Tjiputra, J. F., Kriest, I., Bentsen, M., Bethke, I., et al. (2016). Evaluation of NorESM-OC (versions 1 and 1.2), the ocean carbon-cycle stand-alone configuration of the Norwegian Earth System Model (NorESM1). *Geoscientific Model Development*, *9*(8), 2589–2622. https://doi.org/10.5194/gmd-9-2589-2016

Séférian, R., Berthet, S., Yool, A., Palmiéri, J., Bopp, L., Tagliabue, A., et al. (2020). Tracking improvement in simulated marine biogeochemistry between CMIP5 and CMIP6. *Current Climate Change Reports*, *6*(3), 95–119. https://doi.org/10.1007/s40641-020-00160-0

Sisma-Ventura, G., Or, B. M., Yam, R., Herut, B., & Silverman, J. (2017). pCO_2 variability in the surface waters of the ultra-oligotrophic Levantine Sea: Exploring the air-sea CO_2 fluxes in a fast warming region. *Marine Chemistry*, *196*, 13–23. https://doi.org/10.1016/j.marchem.2017.06.006

Steinfeldt, R., Rhein, M., Bullister, J. L., & Tanhua, T. (2009). Inventory changes in anthropogenic carbon from 1997–2003 in the Atlantic Ocean between 20°S and 65°N. *Global Biogeochemical Cycles*, *23*(3), GB3010. https://doi.org/10.1029/2008GB0033112008GB003311

Stöven, T., & Tanhua, T. (2014). Ventilation of the Mediterranean Sea constrained by multiple transient tracer measurements. *Ocean Science*, *10*(3), 439–457. https://doi.org/10.5194/os-10-439-2014

Takahashi, T. (1961). Carbon dioxide in the atmosphere and Atlantic Ocean water. *Journal of Geophysical Research*, *66*(2), 477–494. https://doi.org/10.1029/JZ066i002p00477

Takahashi, T., Olafsson, J., Goddard, J., Chipman, D., & Sutherland, S. (1993). Seasonal variation of CO_2 and nutrients in the high-latitude surface oceans: A comparative study. *Global Biogeochemical Cycles*, *7*(4), 843–878. https://doi.org/10.1029/93GB02263

Takahashi, T., Sutherland, S. C., Sweeney, C., Poisson, A., Metzl, N., Tillbrook, B., et al. (2002). Global sea-air CO_2 flux based on climatological surface ocean pCO_2, and seasonal biological and temperature effects. *Deep Sea Research Part II: Topical Studies in Oceanography*, *49*(9–10), 1601–1622. https://doi.org/10.1016/S0967-0645(02)00003-6

Takahashi, T., Sutherland, S. C., Wanninkhof, R., Sweeney, C., Feely, R. A., Chipman, D. W., et al. (2009). Climatological mean and decadal change in surface ocean pCO_2 and net sea-air CO_2 flux over the global oceans. *Deep Sea Research Part II: Topical Studies in Oceanography*, *56*(8–10), 554–577. https://doi.org/10.1016/j.dsr2.2008.12.009

Terhaar, J., Frölicher, T. L., & Joos, F. (2022). Observation-constrained estimates of the global ocean carbon sink from Earth system models. *Biogeosciences*, *19*(18), 4431–4457. https://doi.org/10.5194/bg-19-4431-2022

Terhaar, J., Goris, N., Müller, J. D., DeVries, T., Gruber, N., Hauck, J., et al. (2024). Assessment of global ocean biogeochemistry models for ocean carbon sink estimates in RECCAP2 and recommendations for future studies. *Journal of Advances in Modeling Earth Systems*, *16*(3), e2023MS003840. https://doi.org/10.1029/2023MS003840

Thomas, H., Friederike Prowe, A. E., Lima, I. D., Doney, S. C., Wanninkhof, R., Greatbatch, R. J., et al. (2008). Changes in the North Atlantic oscillation influence CO_2 uptake in the North Atlantic over the past 2 decades. *Global Biogeochemical Cycles*, *22*(4), GB4027. https://doi.org/10.1029/2007GB003167

Tjiputra, J. F., Assmann, K., & Heinze, C. (2010). Anthropogenic carbon dynamics in the changing ocean. *Ocean Science*, *6*(3), 605–614. https://doi.org/10.5194/os-6-605-2010

Tjiputra, J. F., Olsen, A., Assmann, K., Pfeil, B., & Heinze, C. (2012). A model study of the seasonal and long–term North Atlantic surface pCO_2 variability. *Biogeosciences*, *9*(3), 907–923. https://doi.org/10.5194/bg-9-907-2012

Tjiputra, J. F., Olsen, A. R. E., Bopp, L., Lenton, A., Pfeil, B., Roy, T., et al. (2014). Long-term surface pCO_2 trends from observations and models. *Tellus B: Chemical and Physical Meteorology*, *66*(1), 23083. https://doi.org/10.3402/tellusb.v66.23083

Tjiputra, J. F., Polzin, D., & Winguth, A. M. (2007). Assimilation of seasonal chlorophyll and nutrient data into an adjoint three-dimensional ocean carbon cycle model: Sensitivity analysis and ecosystem parameter optimization. *Global Biogeochemical Cycles*, *21*(1). https://doi.org/10.1029/2006GB002745

Touratier, F., Goyet, C., Houpert, L., de Madron, X. D., Lefèvre, D., Stabholz, M., & Guglielmi, V. (2016). Role of deep convection on anthropogenic CO_2 sequestration in the Gulf of Lions (northwestern Mediterranean Sea). *Deep Sea Research Part I: Oceanographic Research Papers*, *113*, 33–48. https://doi.org/10.1016/j.dsr.2016.04.003

Ullman, D. J., McKinley, G. A., Bennington, V., & Dutkiewicz, S. (2009). Trends in the North Atlantic carbon sink: 1992–2006. *Global Biogeochemical Cycles*, *23*(4). https://doi.org/10.1029/2008GB003383

Urbini, L., Ingrosso, G., Djakovac, T., Piacentino, S., & Giani, M. (2020). Temporal and spatial variability of the CO_2 system in a riverine influenced area of the Mediterranean Sea, the northern Adriatic. *Frontiers in Marine Science*, *7*, 679. https://doi.org/10.3389/fmars.2020.00679

Vaittinada Ayar, P., Bopp, L., Christian, J. R., Ilyina, T., Krasting, J. P., Séférian, R., et al. (2022). Contrasting projections of the ENSO-driven CO_2 flux variability in the equatorial Pacific under high-warming scenario. *Earth System Dynamics*, *13*(3), 1097–1118. https://doi.org/10.5194/esd-13-1097-2022

Wallace, D. W. (2001). Storage and transport of excess CO_2 in the oceans: The JGOFS/WOCE global CO_2 survey. In *International geophysics* (Vol. 77, p. 489-L). Academic Press. https://doi.org/10.1016/S0074-6142(01)80136-4

Wanninkhof, R. (1992). Relationship between wind speed and gas exchange over the ocean. *Journal of Geophysical Research*, *97*(C5), 7373–7382. https://doi.org/10.1029/92JC00188

Wanninkhof, R. (2014). Relationship between wind speed and gas exchange over the ocean revisited. *Limnology and Oceanography: Methods*, *12*(6), 351–362. https://doi.org/10.4319/lom.2014.12.351

Wanninkhof, R., Park, G. H., Takahashi, T., Sweeney, C., Feely, R., Nojiri, Y., et al. (2013). Global ocean carbon uptake: Magnitude, variability and trends. *Biogeosciences*, *10*(3), 1983–2000. https://doi.org/10.5194/bg-10-1983-2013

Wanninkhof, R., Pickers, P. A., Omar, A. M., Sutton, A., Murata, A., Olsen, A., et al. (2019). A surface ocean CO_2 reference network, SOCONET and associated marine boundary layer CO_2 measurements. *Frontiers in Marine Science*, *6*, 400. https://doi.org/10.3389/fmars.2019.00400

Watson, A. J., Nightingale, P. D., & Cooper, D. J. (1995). Modelling atmosphere—Ocean CO_2 transfer. *Philosophical Transactions of the Royal Society of London. Series B: Biological Sciences*, *348*(1324), 125–132. https://doi.org/10.1098/rstb.1995.0054

Watson, A. J., Schuster, U., Bakker, D. C., Bates, N. R., Corbière, A., González-Dávila, M., et al. (2009). Tracking the variable North Atlantic sink for atmospheric CO_2. *Science*, *326*(5958), 1391–1393. https://doi.org/10.1126/science.1177394

Watson, A. J., Schuster, U., Shutler, J. D., Holding, T., Ashton, I. G., Landschützer, P., et al. (2020). Revised estimates of ocean-atmosphere CO_2 flux are consistent with ocean carbon inventory. *Nature Communications*, *11*(1), 4422. https://doi.org/10.1038/s41467-020-18203-3

Wilkin, J. L., Mansbridge, J. V., & Godfrey, J. S. (1995). Pacific Ocean heat transport at 24 N in a high-resolution global model. *Journal of Physical Oceanography*, *25*(10), 2204–2214. https://doi.org/10.1175/1520-0485(1995)025%3C2204:POHTAI%3E2.0.CO;2

Wimart-Rousseau, C., Wagener, T., Álvarez, M., Moutin, T., Fourrier, M., Coppola, L., et al. (2021). Seasonal and interannual variability of the CO_2 system in the eastern Mediterranean Sea: A case study in the north western Levantine Basin. *Frontiers in Marine Science*, *8*, 649246. https://doi.org/10.3389/fmars.2021.649246

Woolf, D. K., Land, P. E., Shutler, J. D., Goddijn-Murphy, L. M., & Donlon, C. J. (2016). On the calculation of air-sea fluxes of CO_2 in the presence of temperature and salinity gradients. *Journal of Geophysical Research: Oceans*, *121*(2), 1229–1248. https://doi.org/10.1002/2015JC011427

Wright, R. M., Le Quéré, C., Buitenhuis, E., Pitois, S., & Gibbons, M. J. (2021). Role of jellyfish in the plankton ecosystem revealed using a global ocean biogeochemical model. *Biogeosciences*, *18*(4), 1291–1320. https://doi.org/10.5194/bg-18-1291-2021

Yang, M., Bell, T. G., Bidlot, J.-R., Blomquist, B. W., Butterworth, B. J., Dong, Y., et al. (2022). Global synthesis of air-sea CO_2 transfer velocity estimates from ship-based eddy covariance measurements. *Frontiers in Marine Science*, *9*. https://doi.org/10.3389/fmars.2022.826421

Zeng, J., Iida, Y., Matsunaga, T., & Shirai, T. (2022). Surface ocean CO_2 concentration and air-sea flux estimate by machine learning with modelled variable trends. *Frontiers in Marine Science*, *9*, 0–14. https://doi.org/10.3389/fmars.2022.989233

Zunino, P., Pérez, F. F., Fajar, N. M., Guallart, E. F., Ríos, A. F., Pelegrí, J. L., & Hernández-Guerra, A. (2015). Transports and budgets of anthropogenic CO_2 in the tropical North Atlantic in 1992–1993 and 2010–2011. *Global Biogeochemical Cycles*, *29*(7), 1075–1091. https://doi.org/10.1002/2014GB005075

References From the Supporting Information

Andrié, C., Oudot, C., Genthon, C., & Merlivat, L. (1986). CO_2 fluxes in the tropical Atlantic during FOCAL cruises. *Journal of Geophysical Research*, *91*(C10), 11741–11755. https://doi.org/10.1029/JC091iC10p11741

Berthet, S., Séférian, R., Bricaud, C., Chevallier, M., Voldoire, A., & Ethé, C. (2019). Evaluation of an online grid-coarsening algorithm in a global eddy-admitting ocean-biogeochemical model. *Journal of Advances in Modeling Earth Systems*, *11*(6), 1759–1783. https://doi.org/10.1029/2019ms001644

Chien, C. T., Durgadoo, J., Ehlers, D., Keller, D., Koeve, W., Kriest, I., et al. (2022). FOCI-MOPS v1—Integration of marine biogeochemistry within the flexible ocean and climate infrastructure version 1 (FOCI 1) Earth system model. *Geoscientific Model Development*, *15*, 5987–6024. https://doi.org/10.5194/gmd-15-5987-2022

Cossarini, G., Feudale, L., Teruzzi, A., Bolzon, G., Coidessa, G., Solidoro, C., et al. (2021). High-resolution reanalysis of the Mediterranean Sea biogeochemistry (1999–2019). *Frontiers in Marine Science*, *8*, 1537. https://doi.org/10.3389/fmars.2021.741486

Doney, S. C., Lima, I., Feely, R. A., Glover, D. M., Lindsay, K., Mahowald, N., et al. (2009). Mechanisms governing interannual variability in upper-ocean inorganic carbon system and air–sea CO_2 fluxes: Physical climate and atmospheric dust. *Deep Sea Research Part II: Topical Studies in Oceanography*, *56*(8–10), 640–655. https://doi.org/10.1016/j.dsr2.2008.12.006

Döscher, R., Acosta, M., Alessandri, A., Anthoni, P., Arsouze, T., Bergman, T., et al. (2022). The EC-Earth3 Earth system model for the coupled model intercomparison project 6. *Geoscientific Model Development*, *15*(7), 2973–3020. https://doi.org/10.5194/gmd-15-2973-2022

Frajka-Williams, E., Moat, B., Smeed, D., Rayner, D., Johns, W., Baringer, M. O., et al. (2021). Atlantic meridional overturning circulation observed by the RAPID-MOCHA-WBTS (RAPID-Meridional overturning circulation and heatflux array-western boundary time series) array at 26N from 2004 to 2020 (v2020. 1). *British Oceanographic Data Centre-Natural Environment Research Council*. https://doi.org/10.5285/cc1e34b3-3385-662b-e053-6c86abc03444

Gloege, L., Yan, M., Zheng, T., & McKinley, G. A. (2022). Improved quantification of ocean carbon uptake by using machine learning to merge global models and pCO_2 data. *Journal of Advances in Modeling Earth Systems*, *14*(2), e2021MS002620. https://doi.org/10.1029/2021MS002620

Ibánhez, J. S. P., Araujo, M., & Lefèvre, N. (2016). The overlooked tropical oceanic CO_2 sink. *Geophysical Research Letters*, *43*(8), 3804–3812. https://doi.org/10.1002/2016GL068020

Körtzinger, A. (2003). A significant CO_2 sink in the tropical Atlantic Ocean associated with the Amazon River plume. *Geophysical Research Letters*, *30*(24), 2287. https://doi.org/10.1029/2003GL018841

Kriest, I., & Oschlies, A. (2015). MOPS-1.0: Towards a model for the regulation of the global oceanic nitrogen budget by marine biogeochemical processes. *Geoscientific Model Development*, *8*(9), 2929–2957. https://doi.org/10.5194/gmd-8-2929-2015

Landschützer, P., Gruber, N., & Bakker, D. C. (2016). Decadal variations and trends of the global ocean carbon sink. *Global Biogeochemical Cycles*, *30*(10), 1396–1417. https://doi.org/10.1002/2015gb005359

Lefèvre, D. (2010). MOOSE (ANTARES). https://doi.org/10.18142/233

Lefèvre, N., Caniaux, G., Janicot, S., & Gueye, A. K. (2013). Increased CO_2 outgassing in February-May 2010 in the tropical Atlantic following the 2009 Pacific El Niño. *Journal of Geophysical Research: Oceans*, *118*(4), 1645–1657. https://doi.org/10.1002/jgrc.20107

Lefèvre, N., Diverrès, D., & Gallois, F. (2010). Origin of CO_2 undersaturation in the western tropical Atlantic. *Tellus B: Chemical and Physical Meteorology*, *62*(5), 595–607. https://doi.org/10.1111/j.1600-0889.2010.00475.x

Le Quéré, C., Buitenhuis, E. T., Moriarty, R., Alvain, S., Aumont, O., Bopp, L., et al. (2016). Role of zooplankton dynamics for Southern Ocean phytoplankton biomass and global biogeochemical cycles. *Biogeosciences*, *13*(14), 4111–4133. https://doi.org/10.5194/bg-13-4111-2016

Liao, E., Resplandy, L., Liu, J., & Bowman, K. W. (2020). Amplification of the ocean carbon sink during El Niños: Role of poleward Ekman transport and influence on atmospheric CO_2. *Global Biogeochemical Cycles*, *34*(9), e2020GB006574. https://doi.org/10.1029/2020gb006574

Lindsay, K., Bonan, G. B., Doney, S. C., Hoffman, F. M., Lawrence, D. M., Long, M. C., et al. (2014). Preindustrial-control and twentieth-century carbon cycle experiments with the Earth System Model CESM1(BGC). *Journal of Climate*, *27*(24), 8981–9005. https://doi.org/10.1175/jcli-d-12-00565.1

Mauritsen, T., Bader, J., Becker, T., Behrens, J., Bittner, M., Brokopf, R., et al. (2019). Developments in the MPI-M Earth system model version 1.2 (MPI-ESM1. 2) and its response to increasing CO_2. *Journal of Advances in Modeling Earth Systems*, *11*(4), 998–1038. https://doi.org/10.1029/2018ms001400

Nakano, H., Tsujino, H., Hirabara, M., Yasuda, T., Motoi, T., Ishii, M., & Yamanaka, G. (2011). Uptake mechanism of anthropogenic CO_2 in the Kuroshio Extension region in an ocean general circulation model. *Journal of Oceanography*, *67*(6), 765–783. https://doi.org/10.1007/s10872-011-0075-7

Paulsen, H., Ilyina, T., Six, K. D., & Stemmler, I. (2017). Incorporating a prognostic representation of marine nitrogen fixers into the global ocean biogeochemical model HAMOCC. *Journal of Advances in Modeling Earth Systems*, *9*(1), 438–464. https://doi.org/10.1002/2016MS000737

Rödenbeck, C., DeVries, T., Hauck, J., Le Quéré, C., & Keeling, R. F. (2022). Data-based estimates of interannual sea–air CO_2 flux variations 1957–2020 and their relation to environmental drivers. *Biogeosciences*, *19*(10), 2627–2652. https://doi.org/10.5194/bg-19-2627-2022

Séférian, R., Berthet, S., Yool, A., Palmieri, J., Bopp, L., Tagliabue, A., et al. (2020). Tracking improvement in simulated marine biogeochemistry between CMIP5 and CMIP6. *Current Climate Change Reports*, *6*(3), 95–119. https://doi.org/10.1007/s40641-020-00160-0

Séférian, R., Nabat, P., Michou, M., Saint-Martin, D., Voldoire, A., Colin, J., et al. (2019). Evaluation of CNRM Earth-system model, CNRM-ESM2-1: Role of Earth system processes in present-day and future climate. *Journal of Advances in Modeling Earth Systems*, *11*(12), 4182–4227. https://doi.org/10.1029/2019ms001791

Sein, D. V., Koldunov, N. V., Danilov, S., Sidorenko, D., Wekerle, C., Cabos, W., et al. (2018). The relative influence of atmospheric and oceanic model resolution on the circulation of the North Atlantic Ocean in a coupled climate model. *Journal of Advances in Modeling Earth Systems*, *10*(8), 2026–2041. https://doi.org/10.1029/2018ms001327

Stock, C. A., Dunne, J. P., Fan, S., Ginoux, P., John, J., Krasting, J. P., et al. (2020). Ocean biogeochemistry in GFDL's Earth system model 4.1 and its response to increasing atmospheric CO_2. *Journal of Advances in Modeling Earth Systems*, *12*(10), e2019MS002043. https://doi.org/10.1029/2019ms002043

Urakawa, L. S., Tsujino, H., Nakano, H., Sakamoto, K., Yamanaka, G., & Toyoda, T. (2020). The sensitivity of a depth-coordinate model to diapycnal mixing induced by practical implementations of the isopycnal tracer diffusion scheme. *Ocean Modelling*, *154*, 101693. https://doi.org/10.1016/j.ocemod.2020.101693

Yang, S., & Gruber, N. (2016). The anthropogenic perturbation of the marine nitrogen cycle by atmospheric deposition: Nitrogen cycle feedbacks and the 15N Haber-Bosch effect. *Global Biogeochemical Cycles*, *30*(10), 1418–1440. https://doi.org/10.1002/2016gb005421

10.1029/2023GB007862

Erratum

The originally published version of this article contained a typographical error. In the first sentence of the second paragraph of Section 4.3, “between 0.37 and 0.62” should be changed to “between −0.38 and −0.53.” The error has been corrected, and this may be considered the authoritative version of record.